Measuring β^* in SuperKEKB with K Modulation

Paul Thrane[1,2]

[1]Institute of Physics, Norwegian University of Science and Technology, Trondheim, Norway.
[2]CERN, Geneva, Switzerland.

Fall 2018

1 Abstract

SuperKEKB is an asymmetric energy electron positrion collider currently under commissioning in Japan. It aims to achieve a record high luminosity of 8×10^{35} $\mathrm{cm}^{-2}\mathrm{s}^{-1}$, for which accurate measurements of β_y^* are needed. The advanced final focus system is also relevant for studies related to future linear colliders, which similarly need to achieve very high luminosities. Such studies also require accurate measurements of β_y^*. Using both simulations and experimental measurements from SuperKEKB, K modulation is found to be suitable for measuring the β function at the interaction point within 1 %, however it is too uncertain to be used for measuring the displacement of the beam waist away from the interaction point. To work for SuperKEKB, the K modulation technique is generalized to allow known quadrupole fields between the modulated magnets and the interaction point. In addition, the tune shift from a modulated quadrupole is found without assuming a thin lens perturbation, giving a simple method to calculate the tune shift to second order in the quadrupole strength modulation.

2 Acknowledgements

This article is written as an individual project in connection with studies at NTNU, but has been done with considerable assistance from others. Specifically I would like to thank Andreas Wegscheider, Yukiyoshi Onishi, Yoshihiro Funakoshi and Kazuhito Ohmi for the experimental K modulation measurements from HER. Andreas also for a fair amount of help in analyzing and understanding the data. Adam Koval has also helped with analyzing the data, and has been a good discussion partner while preparing him for the continuation of the project. Furthermore, I would like to thank both Felix Carlier and Michael Hofer for help with understanding, applying and modifying K modulation, pointing out that Michael in parallel is doing similar work for the LHC. In addition, Katsunobu Oide has been very helpful, quickly solving several issues encountered while working with SAD. Finally, my supervisor at CERN, Rogelio Tomás, has as always assisted with deep insights, quick and accurate feedback as well as lots of motivation.

CERN-THESIS-2018-300
//2018

Contents

3 Introduction

Currently under commissioning, SuperKEKB is an asymmetric energy electron positron collider at the High Energy Accelerator Research Organization in Japan (KEK) [1]. It is composed of a 7 GeV ring for electrons and a 4 GeV ring for positrons, called the High Energy Ring (HER) and Low Energy Ring (LER), respectively. The accelerator is an upgraded version of KEKB which operated between 1999 and 2010, during which the physics experiment Belle collected an integrated luminosity of 1.04 ab^{-1}, and achieved a record high instantaneous luminosity of 2.11×10^{34} cm^{-2}s^{-1} in 2009 [2]. This made possible the detection of CP violation in B mesons and contributed to the confirmation of the Kobayashi–Maskawa theory [3]. SuperKEKB and the upgraded Belle II aim at a luminosity of 8×10^{35} cm^{-2}s^{-1}, surpassing the previous record by a factor 40. This will allow for an integrated luminosity of 50 ab^{-1}, enabling precision measurements of rare events and thus testing of the Standard Model as well as potentially revealing hints about new physics [4].

This factor 40 increase in luminosity comes mainly from two improvements: increasing the beam current by a factor of 2 and decreasing β_y^* by a factor 20 down to 0.3 mm, β_y^* being the vertical β function at the interaction point (IP). See Table 1 for a list of machine parameters. The luminosity is inversely proportional to β_y^*, and precise measurements along with control of

Table 1: Main parameters of SuperKEKB [1].

		LER (e^+)	HER (e^-)	Unit
Energy	E	4.000	7.007	GeV
Current	I	3.6	2.6	A
Number of bunches		2 500		
Bunch current		1.44	1.04	mA
Circumference	C	3 016.315		m
Emittance	ϵ_x/ϵ_y	3.2/8.64	4.6/12.9	nm/pm
Coupling		0.27	0.28	%
β function at IP	β_x^*/β_y^*	32/0.27	25/0.30	mm
Transverse beam size at IP	σ_x^*/σ_y^*	10.1/48	10.7/62	μm/nm
Crossing angle		83		mrad
Momentum compaction	α_p	3.20	4.55	10^{-4}
Energy spread	σ_δ	7.92	6.37	10^{-4}
Total cavity voltage	V_c	9.4	15.0	MV
Bunch length	σ_z	6.0	5.0	mm
Synchrotron tune	ν_s	-0.0245	-0.0280	
Betatron tune	Q_x/Q_y	44.53/46.57	45.53/43.57	
Energy loss per turn	U_0	1.76	2.43	MeV
Damping time	$\tau_{x,y}/\tau_z$	43.2/22.8	58.0/29.0	msec
Beam-beam parameter	ξ_x/ξ_y	0.0028/0.0881	0.0012/0.807	
Luminosity	L	8×10^{35}		cm^{-2}s^{-1}

this value is therefore important. Several well established techniques exist for measuring the β function, and an overview including comparisons between the methods is found in [5]. Currently in SuperKEKB, β function measurements are done globally using a orbit response matrix method [6]. K modulation directly measures the average β function at a modulated quadrupole by measuring the corresponding tune shift. As a result K modulation is slow for global measurements, but can be used for measuring β^* and has been used to do so in other machines with uncertainty below 1 % [7], [8]. However, it has been shown that the uncertainty of β^* measurements using K modulation grows significantly for small values of β^* [9], raising the question whether K modulation will give accurate measurements in SuperKEKB.

Precise β^* measurements in SuperKEKB are interesting for other machines as well. Future linear colliders like CLIC [10] and ILC [11] require large luminosities on the order of 10^{34} cm^{-2}s^{-1} to meet the demands of the experiments. Such luminosities further require small beam sizes and strong focusing quadrupole magnets with large chromatic aberrations that must be corrected in the final focus systems. For CLIC there are currently two types of focusing systems proposed [12],

one of which is also the baseline for ILC and is being tested at ATF2 [13]. The other focusing system is similar to the one used to correct the chromaticity from the final focusing quadrupoles in LER and HER. This focusing system was tested at FFTB [14], but SuperKEKB will demonstrate the system at smaller IP beam sizes and initial studies have investigated the possibility of reducing β_y^* by a factor 3 beyond the nominal value [15], which would give a further 40 % reduction in the vertical beam size at the IP if chromaticity and nonlinear effects can be properly corrected. Such dedicated studies of the final focus system would make it possible to compare the SuperKEKB system with that used in ATF2, and would require accurate β^* measurements. Figure 1 shows vertical beam size measurements from ATF2, together with the planned beam size for HER and LER, as well as a tentative goal for a possible focus system study. Table 2 displays the chromaticity of the various machines discussed above, approximated using the formula $\xi_y \sim \mathrm{L}^*/\beta_y^*$.

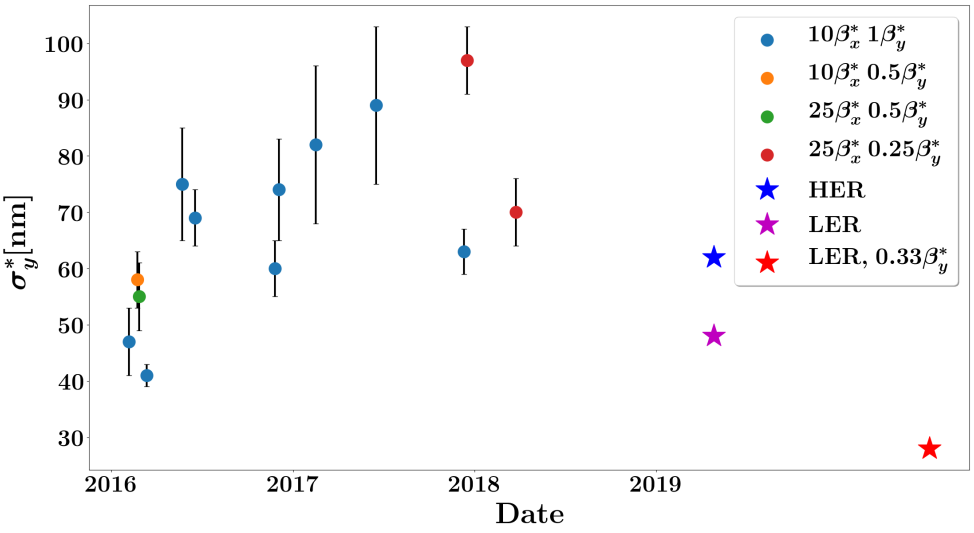

Figure 1: Measured vertical beam sizes in ATF2 [16] for different values of β_x^* and β_y^* as compared to the nominal values. The stars indicate the nominal vertical beam sizes intended for SuperKEKB rings HER and LER. An additional star is added for the case of reduced β_y^* in LER. The values for SuperKEKB are plotted at arbitrary dates.

Table 2: Comparison of chromaticity, ξ_y, in the final focusing quadrupoles for CLIC, ILC, ATF2, FFTB and the Low/High Energy Ring in SuperKEKB.

	L^*[m]	$\beta_y^*[\mu\mathrm{m}]$	$\xi_y \sim (\mathrm{L}^*/\beta_y^*)$
CLIC	3.5	70	50 000
ILC	3.5 /4.1	410	8500 /10 000
ATF2	1	100	10 000
FFTB	0.4	100	4 000
SuperKEKB LER	0.94	270	3 500
SuperKEKB HER	1.41	300	4 700

4 Theory

4.1 Introduction to Transverse Linear Beam Optics

To cover the basics of K modulation, a brief introduction a few concepts of transverse beam optics is required. For a comprehensive treatment of beam dynamics in general see for example [17], from which much of this introduction is based.

In a particle accelerator, charged particles are guided along a predefined path by electromagnetic fields. We define a coordinate system as shown in Figure 2; s denotes the position along the predefined path, while x and y are orthogonal to this path and describe how the particle deviates from the designed trajectory. It is usual to let y point in the vertical direction, and have x in the horizontal plane, assuming the design path also lies in the horizontal plane. The force acting on the particles is given by the Lorentz force

$$\vec{F} = q\vec{E} + q(\vec{v} \times \vec{B}). \tag{1}$$

We assume the charge of the particle q to be the electron charge e. Since the velocity, $\vec{v}$, of the particles is relativistic, it is much more efficient to use magnetic fields $\vec{B}$ to guide the particles than using electric fields $\vec{E}$, and we therefore disregard electric fields. Also, for simplicity we regard only magnetic fields that are transverse to the design trajectory. The force acting on a relativistic particle changes the particles momentum according to

$$\vec{F} = \frac{\mathrm{d}\vec{p}}{\mathrm{d}t} = \frac{\mathrm{d}(m\gamma\vec{v})}{\mathrm{d}t} = m\left(\gamma\frac{\mathrm{d}\vec{v}}{\mathrm{d}t} + \gamma^3\frac{v}{c^2}\frac{\mathrm{d}v}{\mathrm{d}t}\vec{v}\right), \tag{2}$$

with the Lorentz factor γ and the speed of light c. Magnetic fields do not change the speed of the particle, so $\mathrm{d}v/\mathrm{d}t = 0$, and the second term in Equation (2) disappears. For the particle to follow a turn with radius r with constant speed, the acceleration must be v^2/r, together with our assumptions and Equations (1) and (2) this gives

$$evB = \frac{\gamma m v^2}{r}. \tag{3}$$

Assuming $\mathrm{d}z/\mathrm{d}s \ll 1$ where z is either x or y, which is to say that the particle trajectories are close to the design path, we can approximate the curvature $1/r$ as

$$\frac{1}{r} = \frac{\mathrm{d}^2 z}{\mathrm{d}s^2} = z''. \tag{4}$$

Inserting into Equation (3) results in

$$z'' = \frac{eB}{p}. \tag{5}$$

Particles with slightly different momenta p are bent differently by the magnetic fields. However, we shall ignore this effect here and set $p = p_0$, the reference momentum. A full derivation including such chromatic effects can be found in [17]. The magnetic fields in a particle accelerator are specially designed for different purposes, the two main ones being bending the beam to follow the design trajectory and focusing of the beam. The fields that bend the particle beam are constant with respect to z, $B = B_0$, and called dipole fields. The fields that focus or defocus the beam are linearly dependent on z, written as $B = gz$ with the gradient $g = \partial B/\partial z$, these are called quadrupole fields. Ignoring the constant field to get an equation for how the particles deviate from the design trajectory we arrive at

$$z'' + Kz = 0. \tag{6}$$

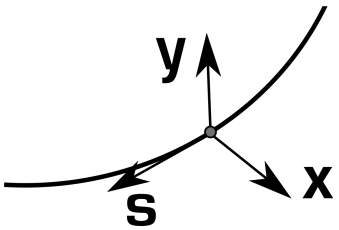

Figure 2: Figure illustrating the coordinates used. The longitudinal distance along the reference orbit is given by s, while the two transverse dimensions are x and y, chosen to be horizontal and vertical respectively.

Here, K is the quadrupole strength coefficient and is defined by $\frac{eg}{p_0}$. Note that both z and k depend on s, and in a circular accelerator K is periodic with the circumference. As a solution to Equation (6) we try

$$z = \sqrt{\epsilon}\omega(s)e^{\pm i\psi(s)}, \tag{7}$$

with a constant amplitude part $\sqrt{\epsilon}$, a varying amplitude factor $\omega(s)$ and a phase $\psi(s)$. Differentiating two times and inserting into Equation (6) gives

$$2\omega'\psi' + \omega\psi'' = 0, \tag{8}$$

$$\omega'' - \omega\psi'\psi' + k\omega = 0. \tag{9}$$

By defining $\beta = \omega^2$ Equation (8) implies

$$(\beta\psi')' = 0, \tag{10}$$

which further means $\beta\psi'$ is a constant which we set to one, resulting in

$$\psi' = \frac{1}{\beta}, \tag{11}$$

$$\psi(s) = \int_{s_0}^{s} \frac{1}{\beta}\mathrm{d}s' + \psi(s_0). \tag{12}$$

Inserting $\omega^2 = \beta$ and $\psi' = 1/\beta$ into Equation (9) gives us a differential equation for β

$$\frac{1}{2}\beta\beta'' - \frac{1}{4}\beta'^2 + \beta^2 K = 1. \tag{13}$$

The solution to Equation (6) now reads

$$z = \sqrt{\epsilon}\sqrt{\beta(s)}\cos(\psi(s) + \psi_0). \tag{14}$$

Every particle in the beam will have its own constant amplitude factor ϵ and starting phase ϕ_0. ϵ of the particles with the largest oscillations is called the emittance, and it has several important properties not covered here, see [17]. With a large number of particles, there will always be some particles with the largest ϵ and a ψ_0 that makes $\cos(\psi(s) + \psi_0) = \pm 1$. Therefore, not considering chromatic effects, β decides the physical extent of the beam due to linear effects.

Given the initial state of a particle z_0 and z_0' we can now find the state at a later point using β and ψ. First define

$$\alpha = -\frac{1}{2}\beta'. \tag{15}$$

The position is then given by

$$z(s) = a\sqrt{\beta(s)}\cos(\psi(s)) + b\sqrt{\beta(s)}\sin(\psi(s)), \tag{16}$$

where , $z'(0) = z_0'$, $\psi(0) = 0$, $\beta(0) = \beta_0$, $\alpha(0) = \alpha_0$ and the values at the end position are given by ψ, β and α. a and b are two coefficients to be determined. The solution can be written as a matrix equation

$$\begin{pmatrix} z(s) \\ z'(s) \end{pmatrix} = \begin{bmatrix} \sqrt{\frac{\beta}{\beta_0}}(\cos\psi + \alpha_0 \sin\psi) & \sqrt{\beta\beta_0}\sin\psi \\ \frac{\alpha_0 - \alpha}{\sqrt{\beta\beta_0}}\cos\psi - \frac{1+\alpha_0\alpha}{\sqrt{\beta\beta_0}}\sin\psi & \sqrt{\frac{\beta_0}{\beta}}(\cos\psi - \alpha_0\sin\psi) \end{bmatrix} \begin{pmatrix} z_0 \\ z_0' \end{pmatrix}. \tag{17}$$

β and α together with $\gamma = (1 + \alpha^2)/\beta$ are known as the optical functions or Twiss functions. If we know how z and z' transform according to some factors C, S, C', S',

$$\begin{pmatrix} z(s) \\ z'(s) \end{pmatrix} = \begin{bmatrix} C & S \\ C' & S' \end{bmatrix} \begin{pmatrix} z_0 \\ z_0' \end{pmatrix}, \tag{18}$$

Equation (17) can be used to find how the optical functions transform, giving

$$\begin{pmatrix} \beta(s) \\ \alpha(s) \\ \gamma(s) \end{pmatrix} = \begin{bmatrix} C^2 & -2CS & S^2 \\ -CC' & CS' + SC' & -SS' \\ C'^2 & -2C'S' & S'^2 \end{bmatrix} \begin{pmatrix} \beta_0 \\ \alpha_0 \\ \gamma_0 \end{pmatrix}. \tag{19}$$

4.2 Tune

In circular accelerators, the phase advance ψ given by Equation (12) around one full turn divided by 2π is called the tune, denoted by Q. For a full turn, the phase advance is therefore $2\pi Q$, and the matrix in Equation (17) becomes

$$\begin{bmatrix} \cos(2\pi Q) + \alpha_0 \sin(2\pi Q) & \beta_0 \sin(2\pi Q) \\ -\gamma_0 \sin(2\pi Q) & \cos(2\pi Q) - \alpha_0 \sin(2\pi Q) \end{bmatrix}, \tag{20}$$

where we have made use of the fact that the optical functions are periodic. We note that the trace of this matrix is equal to $2\cos(2\pi Q)$.

4.3 Quadrupole Magnets

Quadrupole magnets have as the name suggests 4 poles, and as can be seen in Figure 3 they have a positive gradient in one transverse direction and a negative gradient in the other. Thus

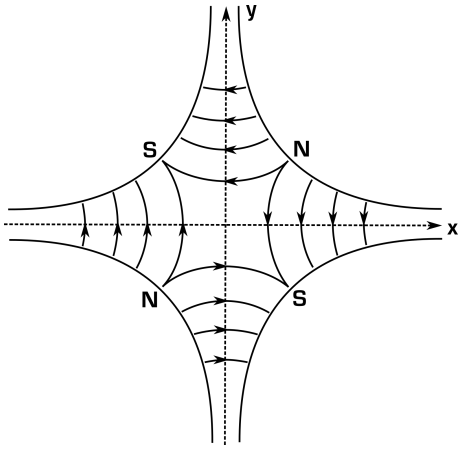

Figure 3: Magnetic field lines inside the cross section of a quadrupole magnet. The magnet is designed such that $\partial B/\partial x = \text{const.}$ and similar for y. Note that if the magnet is focusing in the x direction it will be defocusing in the y direction.

if a quadrupole magnet is focusing in x, it is defocusing in y. To focus the beam in both x and y directions at least two magnets are therefore needed. The longitudinal profile of K along the magnet is usually made to be as constant inside the magnet as possible, and to drop quickly to zero outside the magnet. The parts of the fields that transition to zero from the constant value inside the magnet to the outside are called the fringe fields of the magnet and depend on the particular design. It is usual to neglect the fringe fields and model the magnet strength as a step from zero to a constant value inside the magnet. The first order effect from the fringe fields can be taken into account by making the length of the magnet slightly longer, more details can again be found in [17].

With K constant inside the magnet, Equation (6) is solved by the functions

$$\begin{aligned} C(s) &= \cos(\sqrt{K}s), \\ S(s) &= \frac{1}{\sqrt{K}} \sin(\sqrt{K}s), \end{aligned} \tag{21}$$

if K > 0 i.e. a focusing magnet. And for a defocusing magnet, K < 0, the solutions are

$$\begin{aligned} C(s) &= \cosh(\sqrt{K}s), \\ S(s) &= \frac{1}{\sqrt{K}} \sinh(\sqrt{K}s). \end{aligned} \tag{22}$$

With this notation the state of a particle $z(s)$ and $z'(s)$ can be propagated inside the quadrupole magnet from an initial state z_0 and z_0' using Equation (18). Now the coefficients C and S are given by Equation (21) or (22), and $C' = \mathrm{d}C/\mathrm{d}s$, $S' = \mathrm{d}S/\mathrm{d}s$.

4.3.1 Average β Function in a Quadrupole Magnet

For K modulation we need an expression for the average beta function inside a quadrupole magnet [9]. Given the optical functions at one edge of the magnet β_0, α_0 and γ_0, we have from Equation (19) that β inside the magnet is given by

$$\beta(s) = C^2\beta_0 \pm 2CS\alpha_0 + S^2\gamma_0. \tag{23}$$

Here, the sign in the second term depends on which side of the magnet we know the optical functions, because α changes sign if we propagate in the opposite direction as can be seen from Equation (15). Integrating this expression for β along the full length of the magnet and dividing by the length L, results in

$$\overline{\beta} = \beta_0 u_0 \pm \alpha_0 u_1 + \gamma_0 u_2, \tag{24}$$

where $\overline{\beta}$ is the average beta function and the coefficients u_0, u_1 and u_2 depend on whether the magnet is focusing or defocusing. For a focusing magnet the coefficients are

$$\begin{aligned} u_0 =& \frac{1}{2}\left(1 + \frac{\sin(2\sqrt{K}L)}{2\sqrt{K}L}\right), \\ u_1 =& \frac{\sin^2(\sqrt{K}L)}{KL}, \\ u_2 =& \frac{1}{2K}\left(1 - \frac{\sin(2\sqrt{K}L)}{2\sqrt{K}L}\right). \end{aligned} \tag{25}$$

While for a defocusing magnet they are

$$\begin{aligned} u_0 =& \frac{1}{2}\left(1 + \frac{\sinh(2\sqrt{K}L)}{2\sqrt{K}L}\right), \\ u_1 =& \frac{\sinh^2(\sqrt{K}L)}{KL}, \\ u_2 =& -\frac{1}{2K}\left(1 - \frac{\sinh(2\sqrt{K}L)}{2\sqrt{K}L}\right). \end{aligned} \tag{26}$$

4.4 Drift Section

A section without magnet fields is called a drift section. For the special case of $K = 0$, the coefficients in Equation (21) become $C = 1$, $S = s$, and the derivatives with respect to s become $C' = 0$ and $S' = 1$. A minimum in the beam size is called a waist. Not taking into account chromatic effects, which should be corrected for at the IP, the minimum beam size is given for minimum β function. From Equation (15) we see therefore that $\alpha = 0$ at the waist. Applying Equation (19) we then get expressions for the optical functions a distance l away from a beam waist

$$\begin{aligned} \beta(l) =& \beta_w + \frac{l^2}{\beta_w}, \\ \alpha(l) =& -l\gamma_w = -\frac{l}{\beta_w}, \\ \gamma(l) =& \gamma_w = \frac{1}{\beta_w}. \end{aligned} \tag{27}$$

β_w is the β function at the waist, note that at the waist $\gamma = (1+\alpha^2)/\beta = 1/\beta$. If propagating the optical functions against the motion of the particles, or upstream, the sign in the expression for $\alpha(l)$ must be changed.

4.5 Tune Shift from Modulation of a Quadrupole Magnet

We seek an expression for the change in tune when slightly changing the strength of a quadrupole magnet. This is normally done by assuming the perturbation can be approximated as a thin quadrupole, following the method described in [18]. For a magnet that is short compared to its focal length, $\sqrt{K}L \to 0$, the transfer matrix from Equation (18) becomes

$$\begin{bmatrix} 1 & L \\ \pm KL & 1 \end{bmatrix} \tag{28}$$

where the sign of the lower left element is positive for a defocusing magnet and negative for a focusing magnet. Analogous to geometric light optics, we then make a thin lens approximation by letting the focal length $1/KL$ stay constant while $L \to 0$. The change in quadrupole strength ΔKL is then approximated using such a thin lens matrix as a perturbation. The full turn transfer matrix in Equation (20) can be multiplied by the thin lens matrix, and should then give the full turn matrix but with the new tune

$$\begin{bmatrix} \cos(2\pi Q) + \alpha_0 \sin(2\pi Q) & \beta_0 \sin(2\pi Q) \\ -\gamma_0 \sin(2\pi Q) & \cos(2\pi Q) - \alpha_0 \sin(2\pi Q) \end{bmatrix} \begin{bmatrix} 1 & 0 \\ \pm \Delta KL & 1 \end{bmatrix} =$$

$$\begin{bmatrix} \cos[2\pi(Q+\Delta Q)] + \alpha \sin[2\pi(Q+\Delta Q)] & \beta \sin[2\pi(Q+\Delta Q)] \\ -\gamma \sin[2\pi(Q+\Delta Q)] & \cos[2\pi(Q+\Delta Q)] - \alpha \sin[2\pi(Q+\Delta Q)] \end{bmatrix}. \tag{29}$$

ΔQ is here the change in tune, while the optical functions at the quadrupole before the modulation are β_0, α_0 and γ_0. Doing the matrix multiplication and equating the trace of both sides of the equation results in

$$2\cos(2\pi Q) \pm \beta_0 \Delta KL \sin(2\pi Q) = 2\cos[2\pi(Q+\Delta Q)]. \tag{30}$$

It is then simple to find an expression for the tune shift, if we approximate β_0 with the average β function in the modulated quadrupole, $\overline{\beta}$, we get

$$\Delta Q = \pm \frac{1}{2\pi} \cos^{-1}\left(\cos(2\pi Q) \pm \frac{\overline{\beta} \Delta KL}{2} \sin(2\pi Q) \right) - Q. \tag{31}$$

The sign in front of $\cos^{-1}$ depends on the tune shift, while the sign inside of $\cos^{-1}$ depends on whether the magnet is focusing or defocusing. Equation (30) can be rewritten to

$$\overline{\beta} \approx \beta_0 = \pm \frac{2}{\Delta KL} \left([1 - \cos(2\pi \Delta Q)] \cot(2\pi Q) + \sin(2\pi \Delta Q) \right). \tag{32}$$

Note that for small tune changes this simplifies to

$$\overline{\beta} \approx \pm \frac{4\pi \Delta Q}{\Delta KL}. \tag{33}$$

In the above, the quadrupole modulation was approximated with a thin quadrupole. We show now a slightly different approach that reproduces the same results to linear order in ΔKL, but that also gives the second order tune shift from ΔKL without assuming a thin quadrupole. Let the optical functions at the edge of the magnet be given by β_0, α_0 and γ_0, the one turn matrix starting at the edge of the magnet is then given by Equation (20). The magnet of strength K is then replaced by a magnet of strength $K + \Delta K$ by acting on the one turn matrix with the inverse of the original quadrupole transfer matrix, $\boldsymbol{M}^{-1}(K)$, followed by the transfer matrix of the modulated quadrupole $\boldsymbol{M}(K + \Delta K)$. This gives the one turn transfer matrix $\boldsymbol{T}_{\text{turn}}$ including the modulation

$$\boldsymbol{T}_{\text{turn}} = \begin{bmatrix} \cos(2\pi Q) + \alpha_0 \sin(2\pi Q) & \beta_0 \sin(2\pi Q) \\ -\gamma_0 \sin(2\pi Q) & \cos(2\pi Q) - \alpha_0 \sin(2\pi Q) \end{bmatrix} \boldsymbol{M}^{-1}(K) \boldsymbol{M}(K + \Delta K). \tag{34}$$

These matrices follow from Equation (18), with the coefficients C and S depending on whether the magnet is focusing or defocusing, given by Equation (21) or Equation (22) respectively. The

following steps being similar for both focusing and defocusing magnets, we assume a focusing magnet of length L and have

$$\boldsymbol{M}^{-1}(K) = \begin{bmatrix} \cos(\sqrt{K}L) & -\frac{\sin(\sqrt{K}L)}{\sqrt{K}} \\ \sqrt{K}\sin(\sqrt{K}L) & \cos(\sqrt{K}L) \end{bmatrix},$$
$$\boldsymbol{M}(K+\Delta K) = \begin{bmatrix} \cos(\sqrt{K+\Delta K}L) & \frac{\sin(\sqrt{K+\Delta K}L)}{\sqrt{K+\Delta K}} \\ -\sqrt{K+\Delta K}\sin(\sqrt{K+\Delta K}L) & \cos(\sqrt{K+\Delta K}L) \end{bmatrix}. \tag{35}$$

Calculating $\boldsymbol{M}^{-1}(K)\boldsymbol{M}(K+\Delta K)$ and expanding to second order in ΔK gives

$$\boldsymbol{M}^{-1}(K)\boldsymbol{M}(K+\Delta K) = \begin{bmatrix} 1+a_{11}\Delta K+b_{11}\Delta K^2 & a_{12}\Delta K+b_{12}\Delta K^2 \\ a_{21}\Delta K+b_{21}\Delta K^2 & 1+a_{22}\Delta K+b_{22}\Delta K^2 \end{bmatrix}, \tag{36}$$

where the coefficients a_{ij} and b_{ij} are given by

$$a_{11} = \frac{\sin^2\left(\sqrt{K}L\right)}{2K},$$
$$a_{12} = \frac{L}{2K}\left(1-\frac{\sin\left(2\sqrt{K}L\right)}{2\sqrt{K}L}\right),$$
$$a_{21} = -\frac{L}{2}\left(1+\frac{\sin\left(2\sqrt{K}L\right)}{2\sqrt{K}L}\right),$$
$$a_{22} = -\frac{\sin^2\left(\sqrt{K}L\right)}{2K},$$

$$b_{11} = \frac{1}{8K^2}\left(\sqrt{K}L\sin\left(2\sqrt{K}L\right) - KL^2 - \sin^2\left(\sqrt{K}L\right)\right), \tag{37}$$
$$b_{12} = \frac{1}{16K^{5/2}}\left(3\sin\left(2\sqrt{K}L\right) - 2\sqrt{K}L - 4\sqrt{K}L\cos^2\left(\sqrt{K}L\right)\right),$$
$$b_{21} = \frac{1}{16K^{3/2}}\left(\sin\left(2\sqrt{K}L\right) + 2\sqrt{K}L - 4\sqrt{K}L\cos^2\left(\sqrt{K}L\right)\right),$$
$$b_{22} = \frac{1}{8K^2}\left(-\sqrt{K}L\sin\left(2\sqrt{K}L\right) - KL^2 + 3\sin^2\left(\sqrt{K}L\right)\right).$$

Observe that taking the limit $L \to 0$ all the coefficients become zero to first order in L except $a_{12} = -L$, affirming the thin lens matrix we used earlier in Equation (29). For completeness, the coefficients for a defocusing quadrupole are found the same way and are given by

$$a_{11,def} = -\frac{\sinh^2\left(\sqrt{K}L\right)}{2K},$$
$$a_{12,def} = \frac{L}{2K}\left(1-\frac{\sinh\left(2\sqrt{K}L\right)}{2\sqrt{K}L}\right),$$
$$a_{21,def} = \frac{L}{2}\left(1+\frac{\sinh\left(2\sqrt{K}L\right)}{2\sqrt{K}L}\right),$$
$$a_{22,def} = \frac{\sinh^2\left(\sqrt{K}L\right)}{2K},$$

$$
\begin{aligned}
b_{11,def} &= -\frac{1}{8K^2}\left(\sqrt{K}L\sinh\left(2\sqrt{K}L\right) - KL^2 - \sinh^2\left(\sqrt{K}L\right)\right), \\
b_{12,def} &= \frac{1}{16K^{5/2}}\left(3\sinh\left(2\sqrt{K}L\right) - 2\sqrt{K}L - 4\sqrt{K}L\cosh^2\left(\sqrt{K}L\right)\right), \\
b_{21,def} &= -\frac{1}{16K^{3/2}}\left(\sinh\left(2\sqrt{K}L\right) + 2\sqrt{K}L - 4\sqrt{K}L\cosh^2\left(\sqrt{K}L\right)\right), \\
b_{22,def} &= -\frac{1}{8K^2}\left(-\sqrt{K}L\sinh\left(2\sqrt{K}L\right) - KL^2 + 3\sinh^2\left(\sqrt{K}L\right)\right).
\end{aligned} \tag{38}
$$

Using Equation (36) we can then find an expression for the trace of $\boldsymbol{T}_{\text{turn}}$ in Equation (34)

$$
\begin{aligned}
\text{Tr}\left(\boldsymbol{T}_{\text{turn}}\right) = &\cos(2\pi Q)\left(2 + (a_{11}+a_{22})\Delta K + (b_{11}+b_{22})\Delta K^2\right) \\
&+ \alpha_0\sin(2\pi Q)\left((a_{11}-a_{22})\Delta K + (b_{11}-b_{22})\Delta K^2\right) \\
&+ \beta_0\sin(2\pi Q)\left(a_{21}\Delta K + b_{21}\Delta K^2\right) \\
&+ \gamma_0\sin(2\pi Q)\left(-a_{12}\Delta K - b_{12}\Delta K^2\right).
\end{aligned} \tag{39}
$$

Note that $a_{11} = -a_{22}$ such that $a_{11} + a_{22} = 0$ in Equation (39). From Section 4.2 we know that the trace of $\boldsymbol{T}_{\text{turn}}$ is equal to $2\cos(2\pi Q')$, where $Q' = Q + \Delta Q$ is the new tune after the quadrupole modulation which shifted the tune by ΔQ, and Q is the original tune. To linear order in ΔK we insert the coefficients a_{11}, a_{12}, a_{21}, a_{22} and get

$$
\begin{aligned}
2\cos[2\pi(Q+\Delta Q)] = &\, 2\cos(2\pi Q) - \Delta KL\sin(2\pi Q) \\
&\times\left(\beta_0\frac{1}{2}\left(1 + \frac{\sin\left(2\sqrt{K}L\right)}{2\sqrt{K}L}\right) - \alpha_0\frac{\sin^2\left(\sqrt{K}L\right)}{KL} + \gamma_0\frac{1}{2K}\left(1 - \frac{\sin\left(2\sqrt{K}L\right)}{2\sqrt{K}L}\right)\right).
\end{aligned} \tag{40}
$$

Recognizing the expression for the average β function in a quadrupole from Equation (24) we arrive at

$$
2\cos[2\pi(Q+\Delta Q)] = 2\cos(2\pi Q) - \overline{\beta}\Delta KL\sin(2\pi Q). \tag{41}
$$

When inserting the coefficients for a defocusing magnet, the only change is the sign in front of the second term on the right

$$
2\cos[2\pi(Q+\Delta Q)] = 2\cos(2\pi Q) + \overline{\beta}\Delta KL\sin(2\pi Q). \tag{42}
$$

This is exactly as in Equation (30), assuming $\beta_0 \approx \overline{\beta}$, but now we have included the length of the modulated quadrupole in the calculation.

Returning to Equation (39), we can now find the change to Equation (41) due to the second order terms in ΔK

$$
\begin{aligned}
2\cos[2\pi(Q+\Delta Q)] = &\, 2\cos(2\pi Q) - \overline{\beta}\Delta KL\sin(2\pi Q) \\
&\times\left(1 - \Delta K\frac{\cot(2\pi Q)(b_{11}+b_{22}) + b_{21}\beta_0 + (b_{11}-b_{22})\alpha_0 - b_{12}\gamma_0}{a_{21}\beta_0 + (a_{11}-a_{22})\alpha_0 - a_{12}\gamma_0}\right).
\end{aligned} \tag{43}
$$

Assuming the edge of the quadrupole is a distance L^* away from the beam waist at the IP, the optical functions at the quadrupole edge are given by Equation (27), which results in

$$
\begin{aligned}
2\cos[2\pi(Q+\Delta Q)] = &\, 2\cos(2\pi Q) - \overline{\beta}\Delta KL\sin(2\pi Q) \\
&\times\left(1 - \Delta K\frac{\beta^*\cot(2\pi Q)(b_{11}+b_{22}) + b_{21}L^{*2} - (b_{11}-b_{22})L^* - b_{12}}{a_{21}L^{*2} - (a_{11}-a_{22})L^* - a_{12}}\right).
\end{aligned} \tag{44}
$$

This equation can be used to estimate the error in Equation (32) due to the second order terms of ΔK by inserting the relevant parameter values β^*, L^*, Q, K and L.

4.6 Coupling

Equation (6) describes a situation where the motion in x and y is completely decoupled. However, if the horizontal focusing of a particle is dependent on the vertical position of that particle, such as in a rotated quadrupole, we get a set of coupled equations

$$\begin{aligned} x'' + Kx &= -K_{xy}y, \\ y'' - Ky &= -K_{xy}x, \end{aligned} \tag{45}$$

with K_{xy} given by the skew quadrupole fields. We do not solve these equations here but refer to [17]. Such coupling affects how the vertical and horizontal tunes Q_y and Q_x change when modulating a quadrupole, and therefore gives an error in Equation (31) if coupling is present. Figure 4 shows simulations of how Q_x and Q_y change while modulating a vertically focusing quadrupole magnet in LER when including coupling. The largest deviations happen when the two tunes approach each other and what is called the difference coupling resonance, the width of the corresponding stop-band is called the coupling strength and denoted by $|C^-|$.

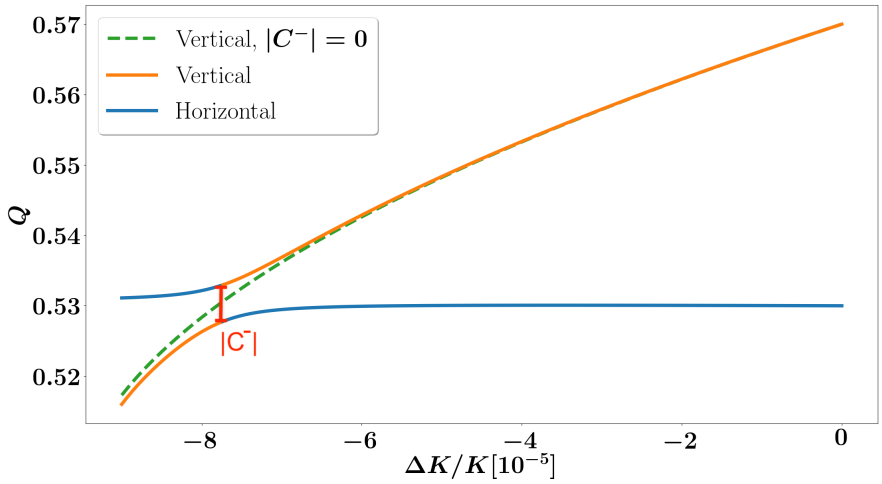

Figure 4: Horizontal and vertical tune when changing the strength of the final vertically focusing quadrupole before the IP. Simulated for the nominal LER lattice with exaggerated coupling to show the effects. The vertical tune without coupling, $|C^-| = 0$, is shown for comparison. The red line indicates how $|C^-|$ can be seen directly from the smallest tune separation.

4.7 Orbit Changes in Sextupole Magnets

The normal transverse fields in a sextupole magnet (as opposed to skew fields) are given by

$$\begin{aligned} B_x &= \frac{1}{2}K_2(x^2 + y^2), \\ B_y &= -K_2xy, \end{aligned} \tag{46}$$

where K_2 is the normal sextupole strength. Therefore, if the beam orbit through the magnet changes by a small horizontal distance δx, the fields become

$$\begin{aligned} B_x &= \frac{1}{2}K_2((x+\delta x)^2 + y^2) = \frac{1}{2}K_2(x^2+y^2) + K_2\delta x x + \frac{1}{2}K_2\delta x^2, \\ B_y &= -K_2(x+\delta x)y = -K_2xy - K_2\delta x y. \end{aligned} \tag{47}$$

Ignoring the second order term in δx, we see that in addition to the original sextupole field the orbit change has introduced a quadrupole field of strength $K_2\delta x$, this effect is called spill-down. Thus, if the orbits are changed when doing K modulation there can be additional tune shifts that

come from sextupole magnets [19]. Given the length of the magnet L_s as well as the β function at the magnet β_s, we can approximate the tune shift using Equation (33)

$$\Delta Q_s \approx \pm \frac{\beta_s K_2 \delta x L_s}{4\pi}. \tag{48}$$

5 Method

5.1 K Modulation

Modulating the strength of a quadrupole will give a tune shift according to Equation (31). As long as the modulation is small, the orbit will stay the same and the tune shift will be only from the change in phase advance through the modulated magnet. Measuring this tune shift and knowing the modulation strength thus gives a direct measurement of the average β function in the modulated quadrupole, given by Equation (32). To find β^* the two quadrupoles closest to the IP are modulated, see Figure 7. Having thereby measured the average β function in these quadrupoles, Equation (24) can be used to relate the optical functions at the magnet end closest to the IP. Propagating the optical functions from the IP, it is then possible to form an analytical expression for β^*. This method has been derived in [9] and is presented below.

Propagating the optical functions from the IP through the final drift of length L^*, the optical functions at the edge of the last quadrupole before the IP are given by Equation (27)

$$\begin{aligned} \beta_0 =& \beta_w + \frac{(L^* \pm w)^2}{\beta_w}, \\ \alpha_0 =& \pm \frac{(L^* \pm w)}{\beta_w}, \\ \gamma_0 =& \frac{1}{\beta_w}. \end{aligned} \tag{49}$$

With $\beta = \beta_w$ at the waist of the beam, and with the waist shifted a distance w downstream of the IP, see Figure 5. The signs depend on whether the magnet is upstream or downstream of the IP. Here and in the following, the upper sign will denote the case where the magnet is upstream, and the lower sign is for the downstream magnet. Inserting into Equation (24) for the average β function in a quadrupole we get

$$\overline{\beta} = \left(\beta_w + \frac{(L^* \pm w)^2}{\beta_w}\right) u_0 + \frac{(L^* \pm w)}{\beta_w} u_1 + \frac{1}{\beta_w} u_2, \tag{50}$$

where the coefficients u_i are given by Equation (25), or (26) depending on if the magnet is focusing or defocusing. For colliders with $\beta^* \ll L^*$ this simplifies to

$$\overline{\beta} = \frac{(L^* \pm w)^2}{\beta_w} u_0 + \frac{(L^* \pm w)}{\beta_w} u_1 + \frac{1}{\beta_w} u_2, \tag{51}$$

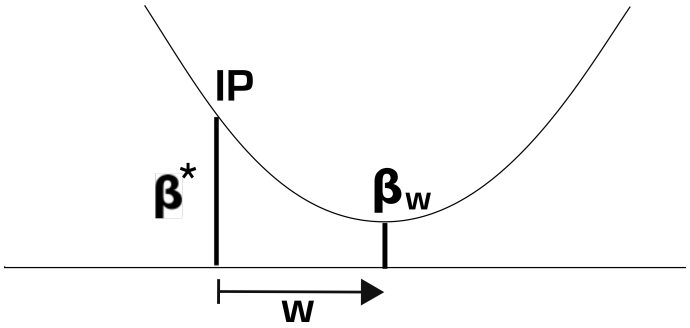

Figure 5: The minimum of the β function is β_w and displaced longitudinally away from the IP a distance w. The β function grows quadratically away from the waist according to Equation (27). w is defined as positive when the waist lies downstream of the IP.

which can be rewritten

$$\beta_w = \frac{1}{\overline{\beta}} \left((L^* \pm w)^2 u_0 + (L^* \pm w) u_1 + u_2 \right). \tag{52}$$

Equating Equation (52) for the magnet upstream and downstream results in

$$\frac{\overline{\beta}_{\text{upstream}}}{\overline{\beta}_{\text{downstream}}} = \frac{(L^* + w)^2 v_0 + (L^* + w) v_1 + v_2}{(L^* - w)^2 u_0 + (L^* - w) u_1 + u_2} = \chi, \tag{53}$$

where the ratio between the average β function in the upstream and downstream quadrupole is defined as χ, which is close to 1 as the focusing system in SuperKEKB is symmetric around the IP. Note however that there is a slight asymmetry in the position and length of the horizontally focusing quadrupoles in HER, see Figure 7. The coefficients u_i for the upstream magnet have been changed to v_i to distinguish them from those for the downstream magnet. Further rewriting leads to a second order equation for w

$$(v_0 - \chi u_0) w^2 + (2L^* v_0 + v_1 + 2\chi L^* u_0 + \chi u_1) w + (L^{*2} v_0 + L^* v_1 + v_2 - \chi L^{*2} u_0 - \chi L^* u_1 - \chi u_2) = 0. \tag{54}$$

Solving for w, Equation (52) can then be used to get a value of β_w for each magnet. Taking the average of these β_w, β^* can then be found by propagating from the waist

$$\beta^* = \beta_w + \frac{w^2}{\beta_w}. \tag{55}$$

5.2 Including Transfer Matrices

If there are quadrupole fields affecting the optical functions in between the final focusing quadrupole and the IP, the method in Section 5.1 cannot be used directly. This is the case for HER in SuperKEKB, see Figure 7. However, the method may be modified to include the effects of these fields by propagating the optical functions past them using Equation (19). Let the optical functions at the end of the quadrupole magnet be given by β_1, α_1 and γ_1. The average β function in the quadrupole is then given by Equation (24)

$$\overline{\beta} = \beta_1 u_0 \pm \alpha_1 u_1 + \gamma_1 u_2, \tag{56}$$

where the sign again depends on if the quadrupole is upstream or downstrem of the IP. To bypass the extra fields between the quadrupole and the IP, a point is chosen that lies between the fields and the IP. Thus, the point is separated from the IP only by a drift of length h, and the optical functions at this point are β_0, α_0 and γ_0. If we know the transfer matrix between this point and the edge of the magnet, the average β function in the magnet can be expressed by β_0, α_0 and γ_0 using Equations (56) and (19)

$$\begin{aligned}
\overline{\beta} =& \beta_1 u_0 \pm \alpha_1 u_1 + \gamma_1 u_2 \\
=& u_0 (C^2 \beta_0 - 2CS\alpha_0 + S^2 \gamma_0) \\
& \pm u_1 (-CC'\beta_0 + (CS' + SC')\alpha_0 - SS'\gamma_0) \\
& + u_2 (C'^2 \beta_0 - 2C'S'\alpha_0 + S'^2 \gamma_0) \\
=& \beta_0 (C^2 u_0 \mp CC' u_1 + C'^2 u_2) \\
& \pm \alpha_0 (\mp 2CS u_0 + (CS' + SC') u_1 \mp 2C'S' u_2) \\
& + \gamma_0 (S^2 u_0 \mp SS' u_1 + S'^2 u_2) \\
=& \beta_0 U_0 \pm \alpha_0 U_1 + \gamma_0 U_2.
\end{aligned} \tag{57}$$

Note that the transfer matrix giving C, C', S and S' is here defined as going from the point closest to the IP and until the magnet edge, regardless of whether the magnet is up- or downstream of the

IP. Here the coefficients U_0, U_1 and U_2 do depend on whether the magnet is up- or downstream of the IP, and are given by

$$\begin{aligned} U_0 =& C^2 u_0 \mp CC' u_1 + C'^2 u_2, \\ U_1 =& \mp 2CS u_0 + (CS' + SC') u_1 \mp 2C'S' u_2, \\ U_2 =& S^2 u_0 \mp SS' u_1 + S'^2 u_2. \end{aligned} \tag{58}$$

From here the procedure is the same as in Section 5.1. Propagating the optical functions from the beam waist near the IP, a distance h away, we get from Equation (27)

$$\begin{aligned} \beta_0 =& \beta_w + \frac{(h \pm w)^2}{\beta_w}, \\ \alpha_0 =& \pm \frac{(h \pm w)}{\beta_w}, \\ \gamma_0 =& \frac{1}{\beta_w}. \end{aligned} \tag{59}$$

With the similar assumption $\beta^* \ll h$, Equations (57) and (59) result in

$$\beta_w = \frac{1}{\beta} \left((h \pm w)^2 U_0 + (h \pm w) U_1 + U_2 \right). \tag{60}$$

Again rewriting and setting the equations of the two magnets equal we get a similar second order equation in w

$$(V_0 - \chi U_0) w^2 + (2hV_0 + V_1 + 2\chi h U_0 + \chi U_1) w + (h^2 V_0 + hV_1 + V_2 - \chi h^2 U_0 - \chi h U_1 - \chi U_2) = 0. \tag{61}$$

As before, χ is the ratio between the average β function in the upstream and downstream quadrupole, and V_i are the coefficients from Equation (58) for the quadrupole upstream of the IP. Having determined w Equation (60) then gives β_w, and the average β_w found for the two magnets is used to calculate β^* from Equation (55).

5.3 Fringe Fields

Equation (31) assumes modulation of a thin quadrupole at a location with a single value of β. Sections 5.1 and 5.2 assume this to correspond to the average β function in a hard edge quadrupole. In practice, magnets also include fringe fields at the edges which scale with the quadrupole modulation but are not taken into account in the above sections. To estimate the error in tune shift due to this approximation, the magnet can be divided into many quadrupole slices, see Figure 6. The tune shift from modulating a single hard edge magnet can then be compared to the combined tune shift resulting from the modulation of all the magnet slices with the same total integrated field strength.

Each quadrupole slice is itself a hard edge magnet and the tune shift is given by Equation (31) with β being the average β function inside the slice. The average of β in slice number i is given by Equation (24)

$$\overline{\beta}_i = u_{0,i}\beta_i - u_{1,i}\alpha_i + u_{2,i}\gamma_i = \begin{bmatrix} u_{0,i} & -u_{1,i} & u_{2,i} \end{bmatrix} \begin{pmatrix} \beta_i \\ \alpha_i \\ \gamma_i \end{pmatrix} = \boldsymbol{A}_i \begin{pmatrix} \beta_i \\ \alpha_i \\ \gamma_i \end{pmatrix}. \tag{62}$$

$\boldsymbol{A}_i$ is here a 1×3 matrix, while β_i, α_i and γ_i are the optical functions at the edge of the slice, see Figure 6. Denoting the 3×3 transfer matrix though quadrupole slice i by $\boldsymbol{T}_i$, the optical functions at the edge of slice $i+1$ are given by

$$\begin{pmatrix} \beta_{i+1} \\ \alpha_{i+1} \\ \gamma_{i+1} \end{pmatrix} = \boldsymbol{T}_i \begin{pmatrix} \beta_i \\ \alpha_i \\ \gamma_i \end{pmatrix} = \prod_{j=0}^{i} (\boldsymbol{T}_j) \begin{pmatrix} \beta_0 \\ \alpha_0 \\ \gamma_0 \end{pmatrix}, \tag{63}$$

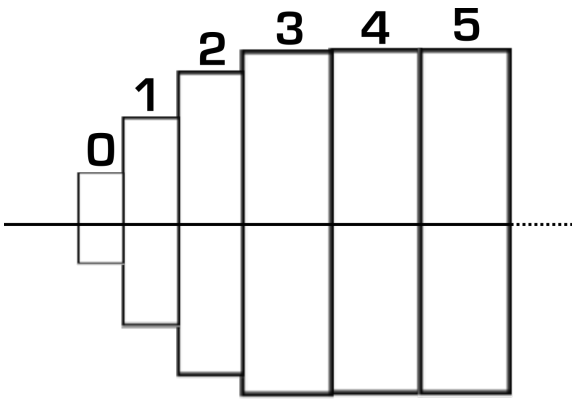

Figure 6: Illustration of several hard edge quadrupole magnets, together modeling a quadrupole with varying field. The slices are numbered, β_0, α_0 and γ_0 corresponds to the beta function at the entrance of slice 0 and so forth.

with β_0, α_0 and γ_0 the optical functions at the start of the first slice. The average β function of slice i follows using Equation (62)

$$\overline{\beta}_i = \boldsymbol{A}_i \begin{pmatrix} \beta_i \\ \alpha_i \\ \gamma_i \end{pmatrix} = \boldsymbol{A}_i \prod_{j=0}^{i-1} (\boldsymbol{T}_j) \begin{pmatrix} \beta_0 \\ \alpha_0 \\ \gamma_0 \end{pmatrix}. \tag{64}$$

Approximating $\beta_0 \Delta KL \approx \sum_{i=0}^{N-1} \overline{\beta}_i \Delta KL_i$ in Equation (31), where N is the number of slices, gives

$$\Delta Q = \pm \frac{1}{2\pi} \cos^{-1} \left(\cos(2\pi Q) \pm \frac{\sin(2\pi Q)}{2} \sum_{i=0}^{N-1} \Delta KL_i \boldsymbol{A}_i \prod_{j=0}^{i-1} (\boldsymbol{T}_j) \begin{pmatrix} \beta_0 \\ \alpha_0 \\ \gamma_0 \end{pmatrix} \right) - Q. \tag{65}$$

Assuming all slices are modulated by the same relative amount δk, Equation (65) can be simplified by defining

$$\boldsymbol{B} = \sum_{i=0}^{N-1} KL_i \boldsymbol{A}_i \prod_{j=0}^{i-1} \boldsymbol{T}_j, \tag{66}$$

which can be found given the strength and length of all the slices. Note that the change in integrated strength ΔKL_i here is exchanged with the total integrated strength KL_i, and that $\Delta KL_i = \delta k KL_i$. This results in

$$\Delta Q = \pm \frac{1}{2\pi} \cos^{-1} \left(\cos(2\pi Q) \pm \frac{\sin(2\pi Q)}{2} \delta k \boldsymbol{B} \begin{pmatrix} \beta_0 \\ \alpha_0 \\ \gamma_0 \end{pmatrix} \right) - Q. \tag{67}$$

5.4 SAD Model

To simulate K modulation measurements in SuperKEKB the computer code Strategic Accelerator Design (SAD) has been used [20]. Supplied with a list of all the elements in a beamline, usually called a lattice, SAD can be used to accurately calculate the optical functions at all element locations along the beamline. Lattices have been supplied by KEK for both HER and LER at SuperKEKB, including detailed representations of the interaction region (IR) that includes fields from the final focusing quadrupoles, detector solenoid, compensation solenoids and corrector magnets [21]. The fields from these elements have been simulated and divided into 1 cm slices that are interleaved throughout the IR model. Figure 7 shows the quadrupole fields near the IP in LER (above) and HER (below). As seen in the figure, there are fields leaking into the electron orbit in HER from the final focusing magnets in LER. When measuring β^* in HER, it is therefore necessary to propagate the β function past these fields using the method described in Section 5.2.

K modulation is simulated by changing the integrated strength of all slices in the IR corresponding to the modulated magnet by the same relative amount. The resulting change in tune is then

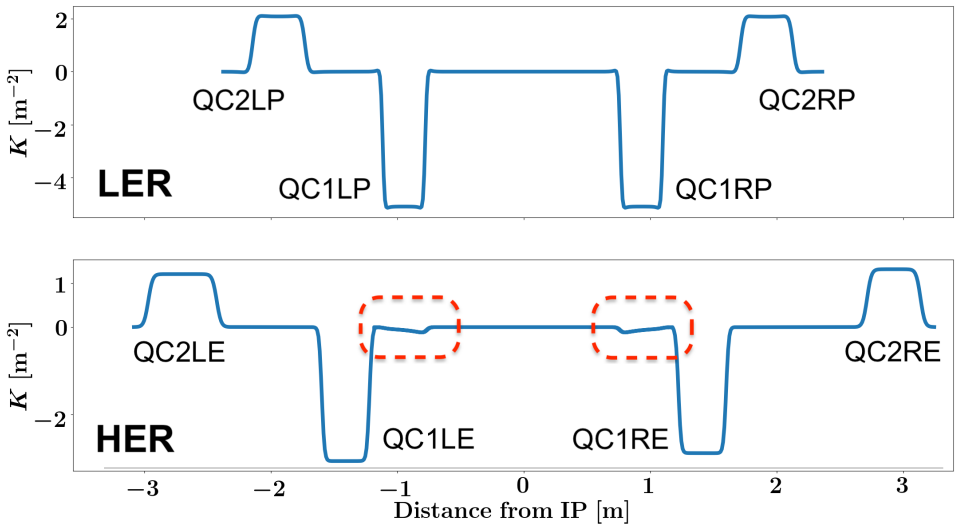

Figure 7: Quadrupole fields in the orbits through the IR of LER (above) and HER (below). The names of the magnets are indicated. Fields from the inner quadrupoles in LER that leak into the HER orbit are pointed out with red rectangles. The focusing system is nearly symmetric, but notice slightly different lengths and placements of horizontally focusing magnets in HER.

calculated by SAD, and is used to estimate β^*. The calculated value can then be compared with the value given by SAD, which takes into account the magnet fringes, coupling and the changing optical functions. Results from these simulations are presented in Section 6.1.

5.5 Simulating Errors

Estimating the uncertainty of the measurement is done by setting uncertainties on the values used to calculate β^*, shown in Table 3. Calculating β^* from the correct values of the parameters gives the measured value. The uncertainty is estimated by finding the spread of β^* when doing the measurement 10 000 times with the model parameters drawn from normal distributions with standard deviations equal to the relevant uncertainties.

Table 3: Uncertainties used for estimating error of β^* measurements. K is the uncertainty in the integrated strength of the modulated quadrupoles, while $K^\dagger$ is the uncertainty in the integrated strength of the quadrupole fields from LER present in the HER orbit. The tune uncertainty is from [22], while typical values have been assumed for the other parameters. Note that the tune uncertainty is for normal turn by turn measurements, while a gated turn by turn measurement for a pilot bunch can be used to get a tune uncertainty of $2 \cdot 10^{-5}$ [22].

Parameter	Uncertainty
L^* [mm]	1
h [mm]	1
Q	$2 \cdot 10^{-4}$
K [relative]	$1 \cdot 10^{-3}$
$K^\dagger$ [relative]	$1 \cdot 10^{-2}$

5.6 Experimental Measurements in HER

During phase 2 of the SuperKEKB commissioning process, K modulation measurements were taken in HER on 5$^{\text{th}}$ of June 2018. One by one, all 4 quadrupoles in the IR were modulated

by ±0.05% and +0.1%. Since we are most interested in β_y^* we will only look at the results from modulation of the quadrupoles closest to the IP, QC1LE and QC1RE. Following each modulation, three sets of turn by turn beam position monitor (BPM) readings were recorded, including three sets for each magnet without modulation as a reference. BPMs read the position of the beam as an average of all the particles in the beam. To get readings corresponding to the phase advances and amplitudes of individual particles a magnet is used to perturb the beam away from the closed orbit. The beam will then oscillate around the closed orbit the same way a individual particle does [23]. The tune is then simply the main frequency component in the measured data. To ensure correct measurement of the tune shift, the tune feedback system was turned off. Design parameters during the measurements are displayed in Table 4 and include $\beta_y^* = 3$ mm. The results from these measurements are presented in Section 6.2

Table 4: Working point and β^* during measurements in HER. The measurements were done on 5^{th} of June 2018, during phase 2 of SuperKEKB commissioning.

Parameter	Value
β_y^* [mm]	3.0
β_x^* [mm]	100
Q_y	43.604
Q_x	45.546

6 Results and Discussion

6.1 Results from Simulations

Simulations of K modulation measurements of β_y^* were done using SAD. Figure 8 shows the deviation of the measurements from the actual value for different values of β_y^* ranging from 3 mm to 90 μm in LER. For all the cases the deviation is less than 0.1 %, and for the nominal case of $\beta_y^* = 270$ μm the deviation is below 0.08 %. As β_y^* decreases towards 90 μm there is a sharp increase in the deviation rising above 0.09 % for $\beta_y^* = 90$ μm.

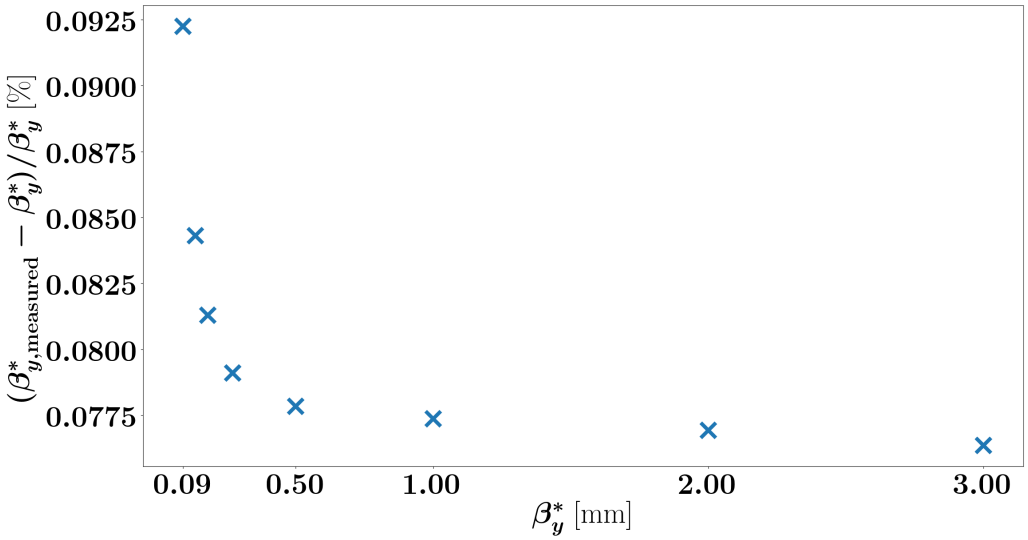

Figure 8: Deviation of the calculated β_y^* as a function of β_y^* in LER, found from simulations using SAD.

There are several assumptions used that could contribute to the deviation of the measured value. Firstly, in Equation (51) it is assumed that $\beta^* \ll L^*$. Even for $\beta_y^* = 3$ mm, a factor

10 above nominal, this term contributes less than 0.005 % and it is therefore insignificant. It is also assumed that there are no orbit changes, and therefore no changes in tune from sextupoles in the ring. For very small values of ΔKL the orbit is not changed in the simulations, while for larger values of ΔKL the deviation of the calculated β_y^* changes less than 0.002 %, which does not account for the observed deviation.

Another simplification is only including the first order of ΔKL in Equation (31). By inserting the relevant parameters for LER in Equation (44) we see that this gives an error of the order 10^{-6} in $\overline{\beta}$, which corresponds to a change in tune of less than 10^{-6}, smaller than the uncertainty of the tune measurement. Comparing the tune shift calculated by SAD and the tune shift found from Equation (31) gives the same size of deviation. It is possible to include the second order terms by using the coefficients from Equation (39) instead of going via the average β function as is done in Section 5.1, however, due to the small error this is not done.

The method further assumes that the horizontal and vertical planes are decoupled. This is true for the lattice used in SAD, where the coupling has been corrected, but for the real machine there will always be some amount of coupling. In this case the impact of the coupling can be reduced by modulating the quadrupoles such that the tune is shifted away from the difference coupling resonance. By adjusting skew quadrupole fields in the ring, the coupling strength in the simulations has been varied and the corresponding deviations of the calculated β_y^* are plotted in Figure 9. Increasing coupling leads to larger deviations, as does smaller β_y^*. For the nominal case

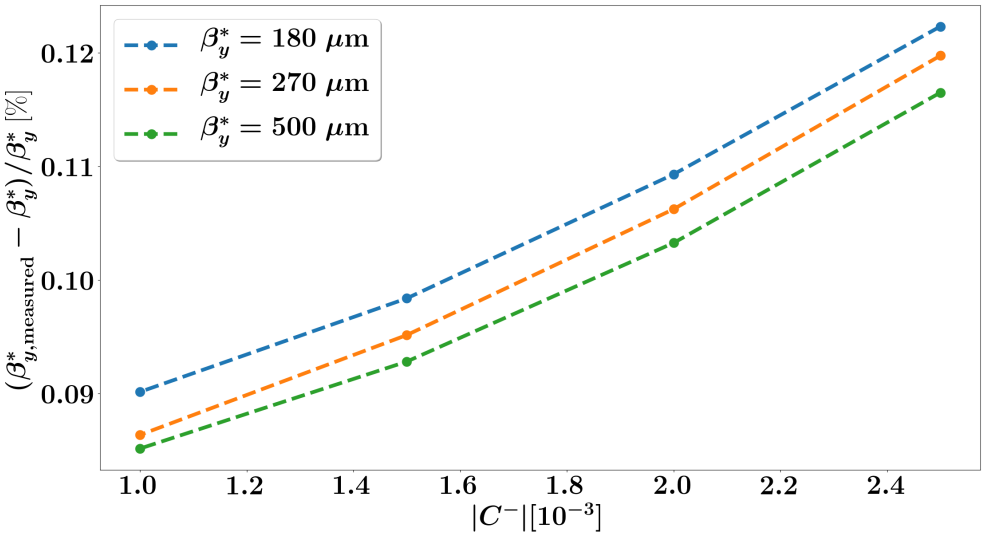

Figure 9: Deviations in the calculated β_y^* for different values of coupling strength in LER. The simulations are done for β_y^* values of 500 μm, 270 μm and 180 μm. The quadrupole modulations are done such that the tune shifts away from the difference coupling resonance.

$\beta_y^* = 270$ μm the deviation increases from 0.08 % at $|C^-| = 0$ to 0.085 % for $|C^-| = 1 \times 10^{-3}$ and until 0.12 % for $|C^-| = 2.5 \times 10^{-3}$. Aiming to achieve a nominal coupling below $|C^-| = 2 \times 10^{-3}$ this gives a deviation below 0.11 % [24], [25]. In [9] a similar increase in deviations of calculated β^* is found to stem from rotations in the modulated quadrupoles. The IR quadrupoles in SuperKEKB include small skew field components by design, which contribute to the observed deviations. Finally, Equation (50) assumes that the modulated quadrupole magnet has a hard edge field profile. Using Equation (67) and Equation (31), the tune shift from modulating the QC1LP quadrupole in LER is calculated using both a hard edge model of the magnet and the sliced SAD model that include the fringe fields. The difference between these two values is shown as a function of β_y^* in Figure 10, and resembles the deviation in β_y^* in Figure 8. However, the exact value of the difference in tune shift is very dependent on the length of the hard edge model, varying between $1 \cdot 10^{-5}$ and $1 \cdot 10^{-4}$ for an uncertainty of 5 mm in w at $\beta_y^* = 90$ μm.

Including uncertainties as described in Section 5.5, the estimated uncertainties in the measured

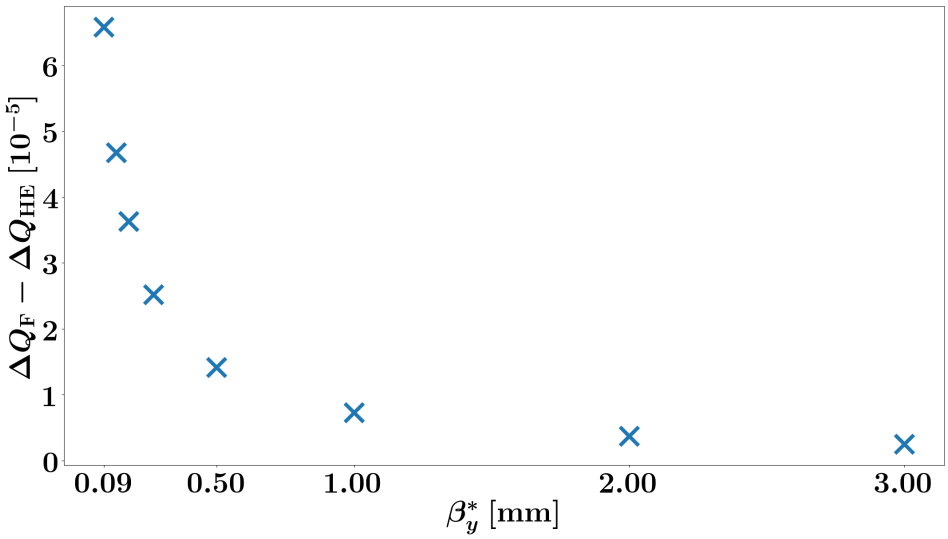

Figure 10: Comparison of tune shifts for different β_y^* calculated using Equation (31) and taking into account the fringes by using Equation (67). The calculations are based on the values for the LER magnet QC1LP, with $\Delta KL/KL = 2 \times 10^{-5}$. The difference is very dependent on the length of the hard edge model, varying between 1×10^{-5} and 1×10^{-4} for an uncertainty of 5 mm in w at $\beta_y^* = 90$ μm.

value for β_w and w are shown in Figures 11 and 12 respectively. The uncertainties in β_w and w are shown as a function of tune measurement accuracy ΔQ and modulated amplitude ΔKL, and are simulated for the nominal LER lattice. The uncertainty in β_w is 0.16 % for an uncertainty

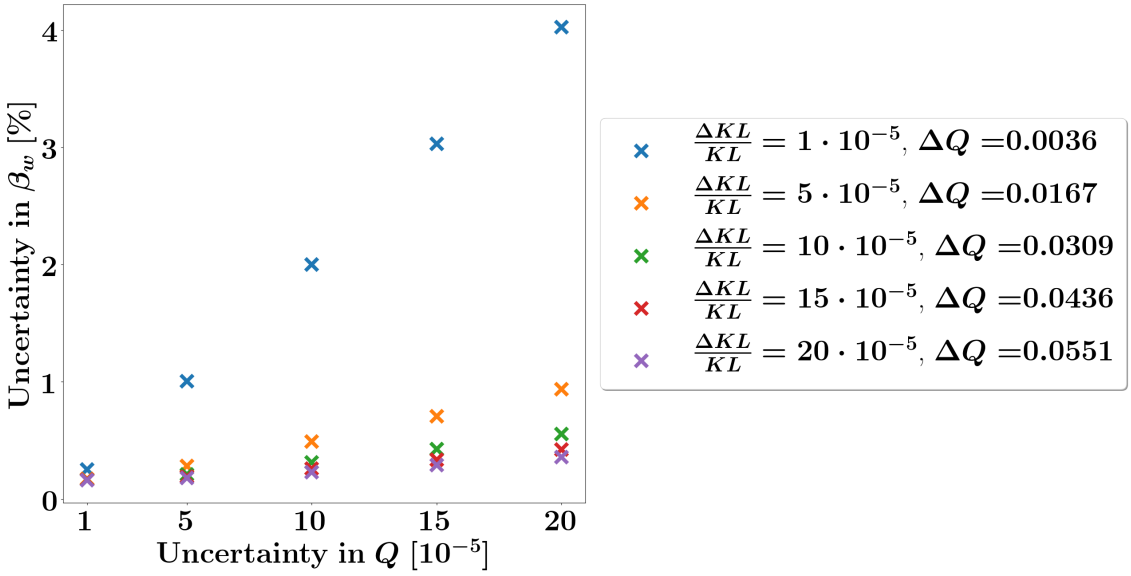

Figure 11: Uncertainty in the β_w measurement in LER for different uncertainties in the tune measurement, as well as for different values of modulation strength ΔKL. Simulated for nominal $\beta_y^* = 270$ μm.

of 1×10^{-5} in tune and $\Delta KL/KL = 2 \times 10^{-4}$ and increases to 0.35 % for a tune uncertainty of 2×10^{-5}, while the uncertainty in w for the same settings increases from 0.8 mm to 1.7 mm. For $\Delta KL/KL = 10^{-5}$, the change in tune approaches the value uncertainty in the tune measurement,

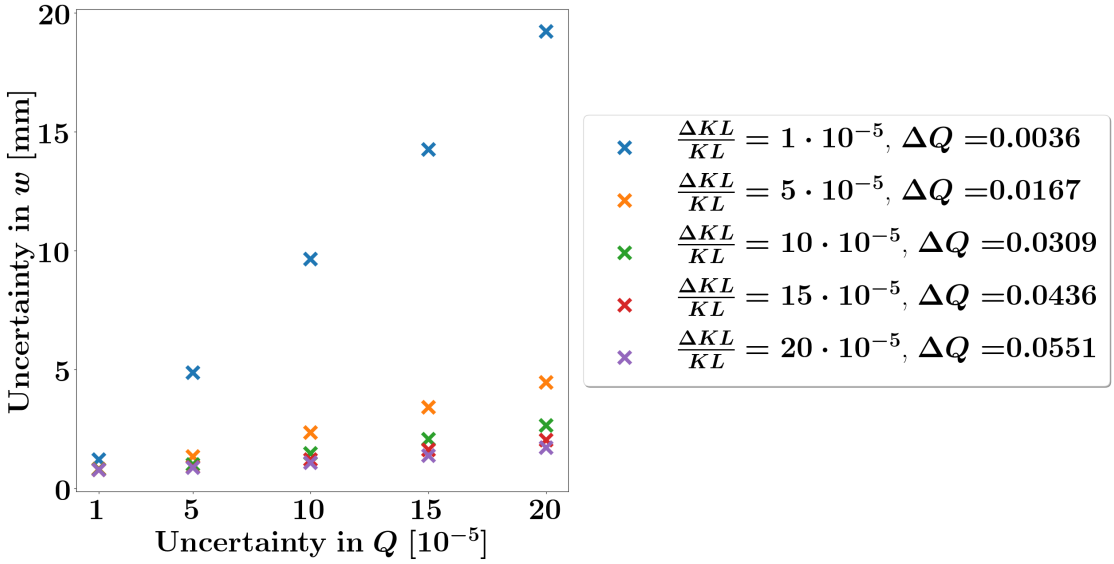

Figure 12: Uncertainty in the w measurement in LER for different uncertainties in the tune measurement, as well as for different values of modulation strength ΔKL. Simulated for nominal $\beta_y^* = 270$ μm.

and the uncertainty in β_w grows from 0.25 % to 4 %, while w goes from 1.2 mm to 20 mm. The large uncertainty in w arises mainly from the uncertainty in the tune measurement and the error in the longitudinal placement of the magnets, assumed to be on the order of 1 mm. In SuperKEKB there are two available tune measurements, a global tune measurement for all stored bunches with resolution 2×10^{-4} and a gated measurement for a pilot bunch with resolution 2×10^{-5} [22]. From Equation (27) it is clear that an uncertainty in w above 1 mm results in a very large uncertainty in β^* when β^* is on the order of 1 mm and below. If $\beta_w = 0.3$ mm and $w = 1$ mm, $\beta^* = (0.3 + 1/0.3)$ mm $= 3.6$ mm. Therefore, K modulation is not suited for measuring w in SuperKEKB. However, the estimated uncertainties for β_w are promising, and can be combined with other methods for determining w, such as measuring the luminosity while varying the longitudinal position of the waist [26].

6.2 Experimental Results from HER

Results from the experimental measurements taken in HER as described in Section 5.6 are presented in Figure 13. The change in the vertical tune is plotted as a function of the relative change in quadrupole strength for the two vertically focusing magnets closest to the IP. Design optics in use during the measurements included $\beta_y^* = 3$ mm, and the uncertainty in the recorded tune measurements are 4×10^{-4} for the modulation of the QC1LE magnet and 2×10^{-4} for the modulation of the QC1RE magnet. Figure 14 shows histograms of the tune measurements by all the BPMs for several settings of the focusing quadrupoles, with different colors used for consecutive sets of turn by turn measurements, displaying a slight jitter in the tune but no visible tune drift. These tune uncertainties were combined with the estimated uncertainties in Table 3 and simulations were used to approximate the uncertainty in the measured values of β_w and w. Figure 13 shows a small deviation from the simulated tune shifts using the design optics, and the measured β function at the waist is $\beta_w = 3.2$ mm with an uncertainty of 0.8 %. The waist itself is measured to be shifted by $w = -4.6$ mm ± 5 mm away from the IP. Figure 15 shows the measured tune shifts again, but this time the lattice used for the simulations has been matched to $\beta_y^* = 3.2$ mm, indicating the close fit for all the measurements.

Figure 16 displays the spectrum of the vertical position measurements from one of the BPMs in HER during the K modulation measurements. The main frequency components correspond to the horizontal and vertical tunes, while the relative amplitude of these frequency components can

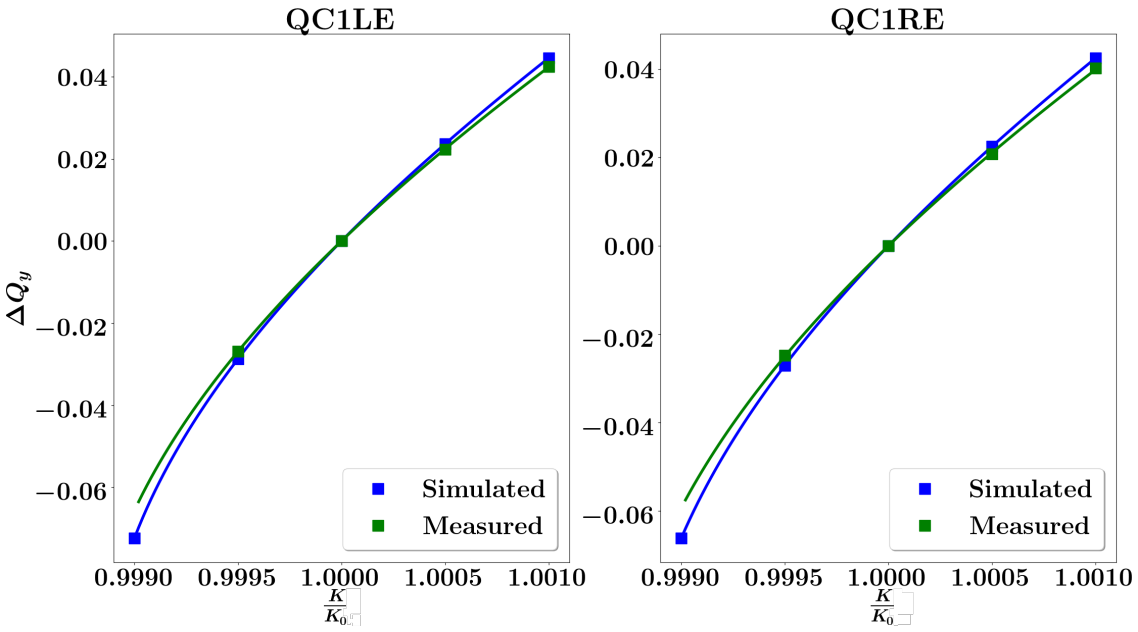

Figure 13: Simulated and measured tune shift when modulating the inner quadrupoles in HER. The simulations are done using the design optics with $\beta_y^* = 3$ mm. The uncertainty in the recorded tune measurements are 4×10^{-4} for the modulation of the QC1LE magnet and 2×10^{-4} for the modulation of the QC1RE magnet. The lines have been made by fitting the average β function and using Equation (31). The integrated strength of the magnets during the measurements were $KL_0 = -1.15$ m^{-1} for QC1LE and $KL_0 = -1.09$ m^{-1} for QC1RE.

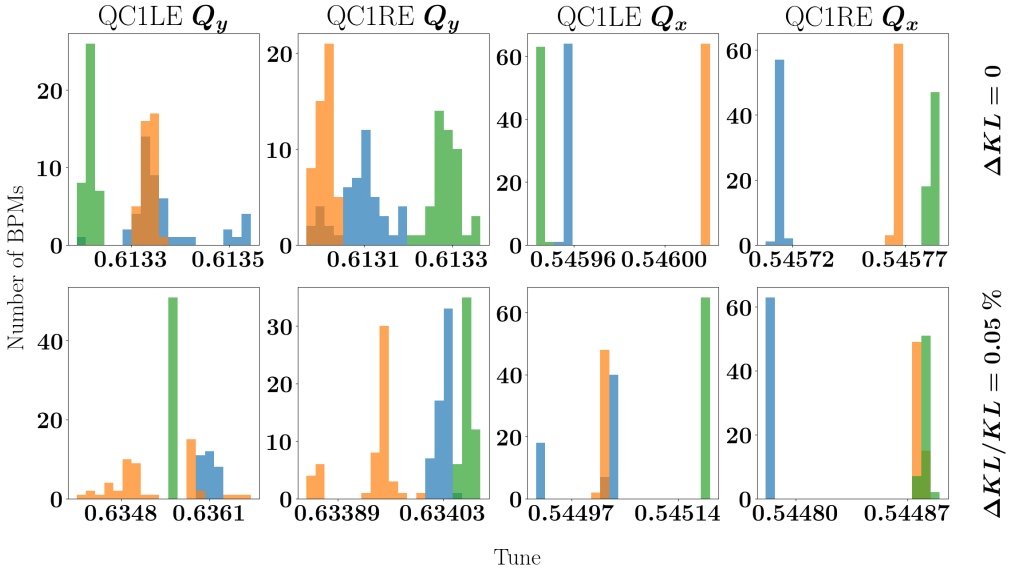

Figure 14: Histograms showing the number of BPMs measuring a certain value of the tune. Three sets of turn by turn measurements were recorded for each setting of the two magnets QC1LE and QC1RE. The colors indicate the sequence of the measurements; blue being first, followed by orange and green last. The histograms on the upper row come from the reference measurements for the magnets with $\Delta KL = 0$, while in the ones on the lower row have $\Delta KL/KL = 0.05$ %. The integrated strength of the magnets during the measurements were $KL_0 = -1.15$ m^{-1} for QC1LE and $KL_0 = -1.09$ m^{-1} for QC1RE.

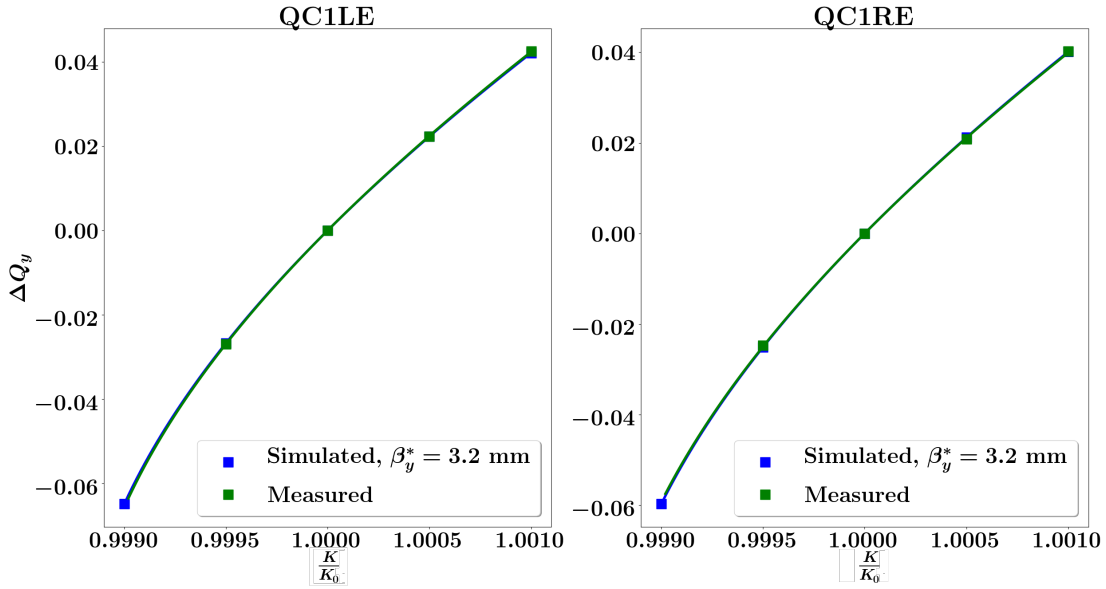

Figure 15: Simulated and measured tune shift when modulating the inner quadrupoles in HER. The simulations are done using $\beta_y^* = 3.2$ mm. The uncertainty in the recorded tune measurements are 4×10^{-4} for the modulation of the QC1LE magnet and 2×10^{-4} for the modulation of the QC1RE magnet. The lines have been made by fitting the average β function and using Equation (31). The integrated strength of the magnets during the measurements were $KL_0 = -1.15$ m^{-1} for QC1LE and $KL_0 = -1.09$ m^{-1} for QC1RE.

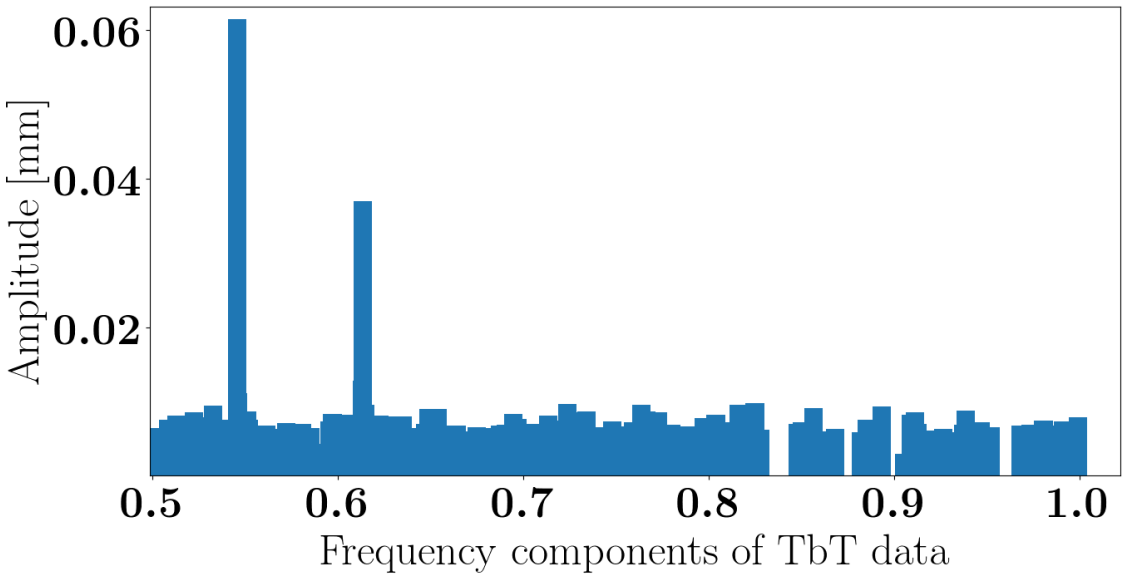

Figure 16: The spectrum of the vertical position measurements from one of the BPMs in HER during the K modulation measurements. The main frequency components of the turn by turn (TbT) data correspond to the horizontal and vertical tunes in the ring.

be used to estimate the coupling in the ring [27]. Coupling estimated from this method is shown in Figure 17. The estimated values for $|C^-|$ vary between vary between 0.001 and 0.003, with the average being a little below 0.002. When modulating the QC1LE magnet by $\Delta KL/KL = -0.05$ % a larger value of $|C^-| = 0.07$ was measured, as well as larger changes in the measured orbits, Figure 19. As shown in Figure 4, coupling starts to have an effect on the tune shifts once the horizontal and vertical tune separation approach the value of $|C^-|$. Figure 18 displays both the

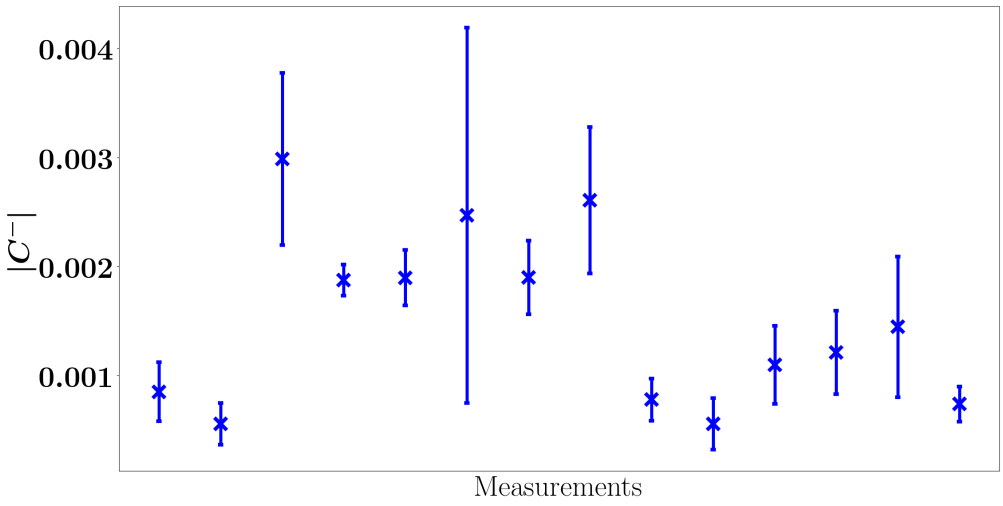

Figure 17: Coupling in HER during the K modulation measurements, estimated from the spectrum of turn by turn data from the BPMs [27]. When modulating the QC1LE magnet by $\Delta KL/KL = -0.05$ % the estimated coupling was a lot larger $|C^-| = 0.07$, this measurement also shows the largest change in the orbit, see Figure 19.

vertical and horizontal tunes during the measurements, and shows that the smallest separation of the tunes is by 0.04, when the magnets are modulated down in strength by $\Delta KL/KL = -0.05$ %. This is a factor 20 larger than the estimated coupling in the ring $|C^-| \approx 0.002$. It should be mentioned that for the nominal parameters presented in Table 1, the tune separation will be 0.04

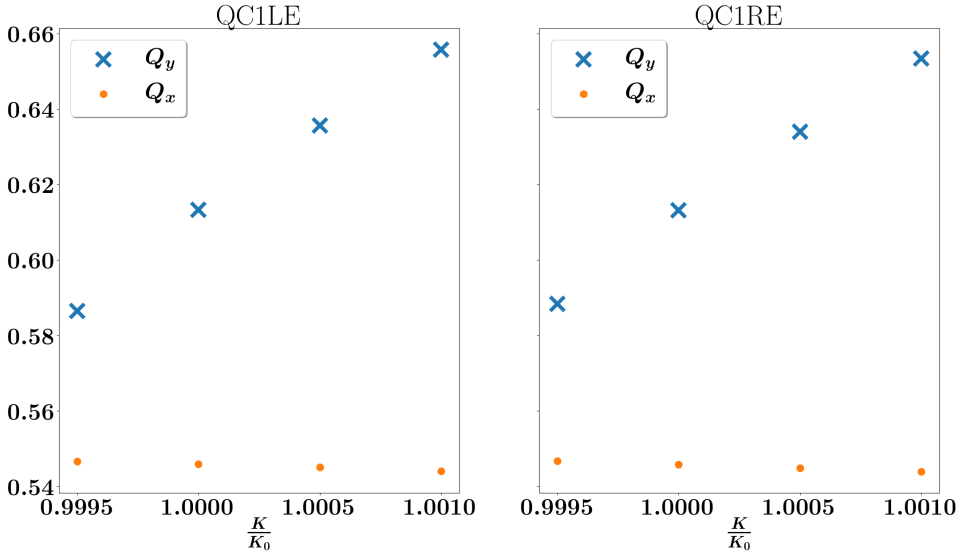

Figure 18: Measured vertical and horizontal tunes while modulating the quadrupole magnets closest to the IP in HER, QC1LE and QC1RE. The smallest separation between the horizontal and vertical tunes is approximately 0.04, which is 20 times larger than the estimated coupling strength during the measurements, $|C^-| \approx 0.002$, see Figure 17. The integrated strength of the magnets during the measurements were $KL_0 = -1.15$ m^{-1} for QC1LE and $KL_0 = -1.09$ m^{-1} for QC1RE.

in both HER and LER, equal to the smallest tune separation during the measurements in HER. Smaller separation than this can be avoided by only modulating up the strength of the quadrupole magnets, as this increases the vertical tune while decreasing the horizontal tune slightly.

However, for the nominal SuperKEKB both the horizontal and vertical tunes will be closer to half integer, at 0.53 and 0.57 respectively. The relative deviation of the β function from the design β function when including errors in the quadrupole gradients K, called beta beating, can be shown to be proportional to $1/\sin(2\pi Q)$ as well as proportional to the value of the β function at the error location [17]. Beta beating and also orbit changes when modulating the focusing magnets

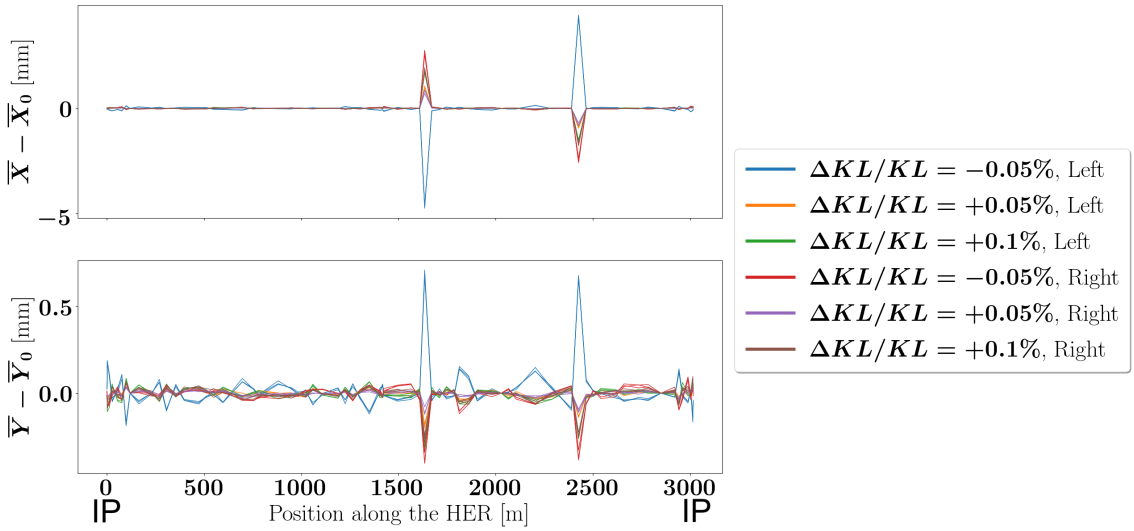

Figure 19: Orbits calculated as the average of all position measurements from turn by turn data taken during the K modulation measurements. The different colors indicate different modulations in the QC1LE and QC1RE magnets, left and right of the IP, respectively. The orbits are plotted as the deviation from the orbits found before modulating the magnets. The two large spikes are believed to be due to malfunctioning BPMs, this is currently under investigation by the monitor group at SuperKEKB [22].

are therefore expected to increase as the fractional part of the tune approaches 0.5. This is seen in Figure 19, where the changes in the mean beam positions in the BPMs are shown when modulating the quadrupoles left and right of the IP. The orbit changes the most when decreasing the magnet strengths, $\Delta KL/KL = -0.05$ %, which brings the vertical tune from 0.613 to 0.586 while the horizontal tune is slightly increased but stays around 0.546. Figure 20 presents the same orbit data, but including only the orbits when modulating up the quadrupole strengths by $\Delta KL/KL = +0.05$ % and $\Delta KL/KL = +0.1$ %, to show more detail. There are two BPMs, MQEAE25 and MQD3E31, that have a factor 10 larger spread in position measurements than the other BPMs, which results in large spikes in Figures 19 and 20. It is believed that there is something wrong with these BPMs, and the issue is being checked by the monitor group at SuperKEKB [22]. Ignoring the two spikes, the orbits change less than 0.05 mm when modulating the strength up by $\Delta KL/KL = +0.1$ %, while modulating the strength down by $\Delta KL/KL = -0.05$ % gives orbit changes of around 0.1 mm at some locations. With Equation (48) it is shown that an orbit displacement of 0.05 mm in HER results in a tune shift from most of the sextupoles smaller than 1×10^{-5}, and thus smaller than the uncertainty of the tune measurements. However, some sextupoles have strong fields in combination with large β functions, giving larger tune shifts. Specifically, there are two sextupoles that give a tune shift of the order ± 0.001 when using Equation (48) for an orbit shift of 0.05 mm, but the tune shifts from these sextupoles have opposite signs and will cancel if the orbit displacements are equal at the two magnets. Any tune shift from the sextupoles should increase linearly with the orbit displacements and affect the measured β_y^*. Figure 21 shows the measured β_y^* for each modulation step $\Delta KL/KL = -0.05$ %, $\Delta KL/KL = +0.05$ % and $\Delta KL/KL = +0.1$ %. The orbit deviations were largest for $\Delta KL/KL = -0.05$ %, but there are no obvious large changes in the measured β_y^*. Moreover, the variations in the measurements are as expected when not taking

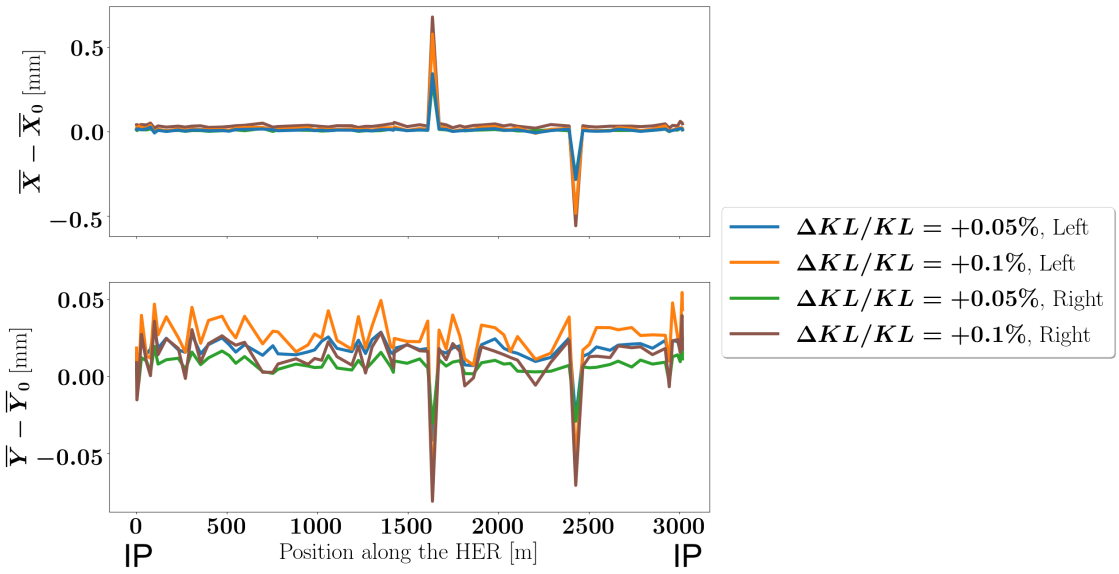

Figure 20: Orbits calculated as the average of all position measurements from turn by turn data taken during the K modulation measurements. The different colors indicate different modulations in the QC1LE and QC1RE magnets, left and right of the IP, respectively. The orbits are plotted as the deviation from the orbits found before modulating the magnets. The two large spikes are believed to be due to malfunctioning BPMs, this is currently under investigation by the monitor group at SuperKEKB [22].

into account any orbit changes in the sextupole magnets. It is therefore assumed that the orbit changes do not affect the measurement, but it is important to investigate if such orbit shifts can affect the K modulation measurements in the nominal machine. Especially since for the nominal machine the smaller β^* results in a larger β function in the final focusing quadrupoles, combined with the tunes being closer to half integer. Such studies are not done here, but a first step would be to analyze the beta beating from the turn by turn data already taken from HER. A natural next step would be to repeat the measurement for a lower β^* during phase 3 of commissioning in SuperKEKB, which is scheduled to start during March 2019.

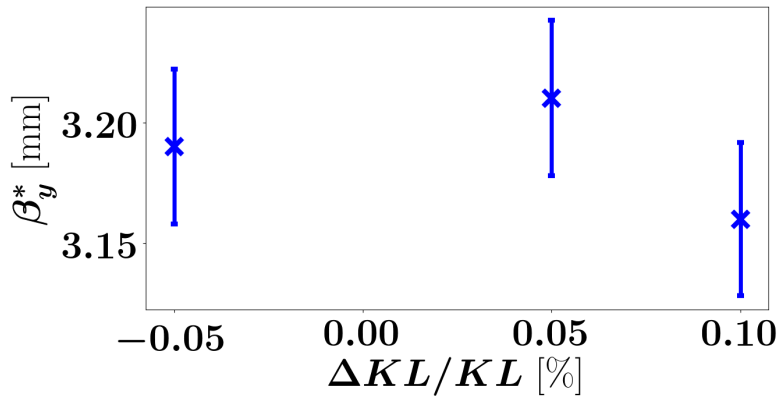

Figure 21: Measured β_y^* as a function of ΔKL for the K modulation measurements in HER. Error bars of 1 % are included, corresponding to the uncertainty estimated from simulations using the measured tune uncertainties and estimated uncertainties in longitudinal placements of the magnets.

7 Conclusion and Further Work

In this paper we evaluate the prospects of using K modulation to measure β^* in SuperKEKB, covering first the needed theory and method. A new technique for finding the tune change from a modulated quadrupole is shown, allowing simple calculation of the second order tune shift due to ΔK. Equation (44) can be used to estimate the size of this second order correction, and can be used also for other accelerators. Furthermore, an extension to the standard K modulation method permits known fields to be located between the modulated quadrupole and the IP, generalizing the technique. This allows the method to be used in HER, where fields from magnets in LER are located between the final focusing quadrupoles and the IP. Also, a method to estimate the effects of fringe fields in the modulated magnets is developed and used to estimate the error from the hard edge magnet assumption.

K modulation measurements in SuperKEKB are motivated by the need for accurate β^* measurements for achieving the extremely high luminosity goal of SuperKEKB, but also by the possibility of doing dedicated focus system studies that will give valuable input to future linear collider projects. From both simulations and experimental results from HER, it is found that K modulation is suitable for measuring β_w in SuperKEKB within 1 %, while the measurement of the position of the beam waist, w, is not accurate enough, varying by several mm. One possibility is therefore to combine K modulation with a set of luminosity measurements while varying the position of the beam waist, a common technique used for placing the beam waist at the IP. The main contributions to the uncertainty are found to come from the uncertainty of the tune measurements, as well as in the uncertainty of the longitudinal placement of the modulated quadrupoles. The measurements from HER give $\beta_y^* = 3.2$ mm ± 0.8 % for a design optics of $\beta_y^* = 3.0$ mm, indicating 7 % beta beating in the machine during phase 2 of commissioning. This should be confirmed by calculating the beta beating from other methods available using the acquired data [5]. Magnet fringes and second order terms in ΔK are found to contribute less than the uncertainty in the tune for the K modulation measurement in HER. Due to measuring the same β_y^* for different modulation steps where the orbit shifts vary significantly, it is assumed that these orbit shifts have not affected the β_y^* measurement. However, the nominal machine parameters include tunes closer to half integer and larger β functions in the modulated quadrupoles, which both could increase the orbit displacements. A first step to investigate these effects is to calculate the beta beating for the different modulation steps using the data already acquired, while a further goal should be to do another K modulation measurement in SuperKEKB for a smaller value of β_y^*.

References

[1] K. Akai, K. Furukawa, and H. Koiso, "Superkekb collider," *Nuclear Inst. and Methods in Physics Research, A*, vol. 907, pp. 188–199, 2018.

[2] T. Abe et. al., "Achievements of kekb," *Progress of Theoretical and Experimental Physics*, vol. 2013, no. 3, pp. 3A001–0, 2013.

[3] F. Takasaki, "The discovery of cp violation in b-meson decays," *Proceedings of the Japan Academy. Series B, Physical and biological sciences*, vol. 88, no. 7, 2012.

[4] G. Casarosa, "The belle ii experiment," *Journal of Physics: Conference Series*, vol. 556, no. 1, 2014.

[5] R. Tomás, M. Aiba, A. Franchi, and U. Iriso, "Review of linear optics measurement and correction for charged particle accelerators," *Physical Review Accelerators and Beams*, vol. 20, no. 5, 2017. [Online]. Available: https://doaj.org/article/c265f60b58a04a80a055fc00e893395d

[6] Y. Ohnishi, H. Sugimoto, A. Morita, H. Koiso, K. Oide, K. Ohmi, D. Zhou, Y. Funakoshi, N. Carmignani, S. M. Liuzzo, M. E. Biagini, M. Boscolo, and S. Guiducci, "Optics measurements and corrections at the early commissioning of SuperKEKB," no. CERN-ACC-2017-0039, p. THPOR007, May 2016. [Online]. Available: http://cds.cern.ch/record/2268264

[7] M. Kuhn, V. Kain, A. Langner, and R. Tomás, "First k-modulation measurements in the lhc during run 2," 2016.

[8] T. Persson, F. Carlier, J. C. de Portugal, A. G.-T. Valdivieso, A. Langner, E. Maclean, L. Malina, P. Skowronski, B. Salvant, R. Tomás, and A. G. Bonilla, "Lhc optics commissioning: A journey towards 1% optics control," *Physical Review Accelerators and Beams*, vol. 20, no. 6, 2017. [Online]. Available: https://doaj.org/article/6b1de29b7e594532bf50086db5a02292

[9] F. Carlier and R. Tomás, "Accuracy and feasibility of the β^* measurement for lhc and high luminosity lhc using k modulation," *Physical Review Accelerators and Beams*, vol. 20, no. 1, 2017. [Online]. Available: https://doaj.org/article/b50b17ab79504b2b9af075255d5cf744

[10] The CLIC and CLICdp collaborations et al., "Updated baseline for a staged Compact Linear Collider," *arXiv:1608.07537 [hep-ex, physics:physics]*, Aug. 2016, arXiv: 1608.07537. [Online]. Available: http://arxiv.org/abs/1608.07537

[11] G. Aarons *et al.*, "ILC Reference Design Report Volume 1 - Executive Summary," 2007.

[12] H. G. Morales and R. Tomás García, "Final-focus systems for multi-TeV linear colliders," *Physical Review Special Topics - Accelerators and Beams*, vol. 17, no. 10, Oct. 2014. [Online]. Available: https://link.aps.org/doi/10.1103/PhysRevSTAB.17.101001

[13] S. Kuroda, "ATF2 for Final Focus Test Beam for Future Linear Colliders," *Nuclear and Particle Physics Proceedings*, vol. 273-275, pp. 225–230, Apr. 2016. [Online]. Available: https://linkinghub.elsevier.com/retrieve/pii/S2405601415005192

[14] Alexandrov, V. A. et al., "Results of final focus test beam," *Conf.Proc.*, vol. C950501, pp. 2742–2746, 1996.

[15] P. Thrane, "Probing LINEAR Collider Final Focus Systems in SuperKEKB," CERN, Geneva, Tech. Rep. CERN-ACC-2017-0052. CLIC-Note-1077, Jun 2017. [Online]. Available: https://cds.cern.ch/record/2276026

[16] F. Plassard, "Optics optimization of longer l* beam delivery system designs for clic and tuning of the atf2 final focus system at ultra-low β^* using octupoles," Ph.D. dissertation, 2018, thèse de doctorat dirigée par Bambade, Philip et Tomas, Rogelio Physique des accélérateurs Paris Saclay 2018. [Online]. Available: http://www.theses.fr/2018SACLS122

[17] H. Wiedemann, *Particle Accelerator Physics*, 4th ed., ser. Graduate Texts in Physics. Springer, 2015.

[18] M. Minty and F. Zimmermann , *Measurement and Control of Charged Particle Beams.* Springer, 2003.

[19] L. van Riesen-Haupt, J. C. de Portugal, E. Fol, A. Seryi, and R. Tomás, "K-Modulation Developments via Simultaneous Beam Based Alignment in the LHC," in *Proc. of International Particle Accelerator Conference (IPAC'17), Copenhagen, Denmark, May, 2017*, ser. International Particle Accelerator Conference, no. 8. Geneva, Switzerland: JACoW, May 2017, paper TUPVA042, pp. 2159–2162, https://doi.org/10.18429/JACoW-IPAC2017-TUPVA042. [Online]. Available: http://jacow.org/ipac2017/papers/tupva042.pdf

[20] "Strategic Accelerator Design (SAD)." [Online]. Available: http://acc-physics.kek.jp/SAD/

[21] "SuperKEKB Design Report, preliminary." [Online]. Available: https://kds.kek.jp/indico/event/15914/

[22] Yukiyoshi Onishi, private communications.

[23] L. Malina, J. C. de Portugal, T. Persson, P. Skowroński, R. Tomás, A. Franchi, and S. Liuzzo, "Improving the precision of linear optics measurements based on turn-by-turn beam position monitor data after a pulsed excitation in lepton storage rings," *Physical Review Accelerators and Beams*, vol. 20, no. 8, 2017. [Online]. Available: https://doaj.org/article/221fe69b99b540299385c48895268f2c

[24] H. Koiso, A. Morita, Y. Ohnishi, K. Oide, and H. Sugimoto, "A Scheme for Horizontal-vertical Coupling Correction at SuperKEKB," *Conf. Proc.*, vol. C1205201, pp. 1203–1205, 2012.

[25] Y. Ohnishi, Y. Funakoshi, H. Koiso, A. Morita, K. Oide, and H. Sugimoto, "Optics correction and low emittance tuning at the phase 1 commissioning of superkekb," 2017.

[26] A. Morita, "Status of SuperKEKB phase-2 commissioning," *ICHEP 2018*. [Online]. Available: https://indico.cern.ch/event/686555/contributions/2962552/attachments/1681111/2700857/ichep2018_KEK_A.Morita.pdf

[27] A. Franchi, R. Tomas Garcia, and G. Vanbavinkhove, "Computation of the Coupling Resonance Driving term f1001 and the coupling coefficient C from turn-by-turn single-BPM data." May 2010. [Online]. Available: http://cds.cern.ch/record/1264111